Erik Gerstl BSc

Design and Validation of a Spectroscopy Chamber for the Development of Formulations and PAT Tools used in the Pharmaceutical HME Process

MASTER'S THESIS

to achieve the university degree of

Diplom-Ingenieur

Master's degree programme: Chemical and Process Engineering

submitted to

Graz University of Technology

Supervisor

Assoc.Prof. DI Dr. Heidrun Gruber-Wölfler
Institute of Process and Particle Engineering

Co-supervisors

DI Johannes Poms
DI Dr. Daniel Treffer

Graz, September 2018

AFFIDAVIT

I declare that I have authored this thesis independently, that I have not used other than the declared sources/resources, and that I have explicitly indicated all material which has been quoted either literally or by content from the sources used. The text document uploaded to TUGRAZonline is identical to the present master‘s thesis.

Date

Signature

Acknowledgements

At first, I want to thank Daniel Treffer, CEO and founder of MeltPrep GmbH and principal of the spectroscopy chamber, for entrusting this project to me. I accompanied him to the PBP World Meeting 2018, had many productive and funny meetings and learned a lot about product development and the importance of creativity and innovation.

I also want to give thanks to my supervisor Johannes Poms for pointing me always into the right direction with his patience and knowledge. With his huge competence in spectroscopic analysis, data interpretation and general physics he gave me big support in my work and had let me gain a lot of scientific experience.

Moreover, I want to thank Heidrun Gruber-Wölfler for being my professor and her helpful tips and hints and Manuel Kreimer for sharing his knowledge in polymer science and HME with me. Thanks to the ColVisTec AG team for giving me the possibility to do tests at their headquarter. They supported me with their professional knowledge and suggestions for improvement.

My sincere thanks also go to my girlfriend Christina, my roommates and the kappa clique. You have supported me in hard times and enriched my student life.

Finally, I want to express my gratitude to my whole family and especially to my parents and grandparents, which have always trusted in me and supported me in every possible way.

Abstract

This thesis investigates a new way of generating spectroscopic reference data sets on polymer melts containing active pharmaceutical ingredient (API). Process analytical technology (PAT) is used to monitor and control the product quality in the pharmaceutical hot melt extrusion (HME) process. To avoid the consumption of high amounts of material and the associated material costs during the design and calibration of spectroscopic PAT methods, it was necessary to develop a tool providing similar conditions to the HME process with less material consumption. The idea of the spectroscopy chamber arose, giving the possibility to install up to two process sensors with equipment specific ports (Dynisco thread 1/2"-20 UNF-2B). The chamber allows transmission and reflectance measurements on polymer melts requiring just a few grams of starting material. The basis of the spectroscopy chamber is formed by the vacuum compression molding (VCM) tool, commercialized by MeltPrep GmbH. With this technology, it is possible to achieve variable melt temperatures and an adjustable probe distance during single measurements. Furthermore, the occurrence of bubbles in the polymer melt is prevented. Additionally, there is a simplified cleaning procedure, so further experiments can be initiated in short time.

The chamber was tested with pure materials (Eudragit® E, EVA28), giving similar results as the UV/Vis, NIR, Raman spectra from literature or reference materials. With the new set-up it is possible to see the influence of degradation via UV/Vis spectroscopy and differences in solid and molten state using Raman spectroscopy. Estriol embedded in EVA28 was used to test the ability of detecting an API. The varying concentrations are easily recognizable in the respective absorption spectrum and it is possible to build a chemo-metric model based with the recorded data. Even 0.005% API content can be identified, and the resultant molar absorption coefficient assorts well with the known reference. After some practicing it is possible measuring up to one sample per hour, cleaning, heat up and cool down included.

The spectroscopy chamber is a simple complement for studies on HME, especially for the design of possible PAT methods. Furthermore, its purpose can be extended

to all kinds of spectroscopic studies on thermoplastics used in polymer and pharmaceutical industries, because it gives a standardized method of spectroscopic material characterization adapted for polymer melts. Experiments can be carried out very fast and with low material usage. It is even possible to analyze the same sample with different methods by changing the probes without changing the inner lying sample.

Kurzfassung

Diese Arbeit befasst sich mit der Entwicklung einer neuen Methode, um Referenzdaten durch spektroskopische Analyse von Wirkstoff haltigen Polymerschmelzen zu generieren. In der pharmazeutischen Heiß-Schmelz-Extrusion (HME) wird die prozessanalytische Technologie (PAT) verwendet, um die Produktqualität laufend zu überwachen und zu regeln.

Das Auslegen und Kalibrieren spektroskopischer PAT Methoden war bisher mit einem hohen Material- und Kostenaufwand verbunden. Deshalb war es notwendig ein Tool zu entwickeln, das ähnliche Bedingungen wie in der HME schafft und gleichzeitig den Materialaufwand minimiert. Damit war die Idee der Spektroskopie Kammer geboren, welche bis zu zwei Prozesssonden (ausgestattet mit einem spezifischem Dynisco Gewinde) aufnehmen kann und mit nur wenigen Gramm Ausgangsmaterial Transmissions- sowie Reflektionsmessungen ermöglicht. Die Basis der Kammer bildet das vacuum compression molding (VCM) Tool der Firma MeltPrep GmbH. Diese Technologie ermöglicht es, die Temperatur der Schmelze und den Abstand der Sonden während der Messung zu variieren. Zusätzlich wird das Auftreten von Blasen in der Schmelze verhindert und der Reinigungsaufwand minimiert.

In der Kammer wurden reine Polymere (Eudragit® E, EVA28) vermessen und mit bekannten Daten aus Referenzmessungen verglichen. Mittels UV/Vis Spektroskopie war es möglich Degradation der Probe festzustellen und mittels Raman Spektroskopie den Unterschied zwischen Feststoff und Schmelze zu beobachten. Um die Möglichkeiten der API Erkennung zu testen, wurde als Testsystem Estriol eingebettet in EVA28 verwendet. Unterschiedliche API Konzentrationen bildeten sich deutlich in den jeweiligen Absorptionsspektren ab und es konnte ein chemometrisches Modell aus den generierten Daten gebildet werden. Wirkstoff konnte selbst in der 0.005% API Probe noch identifiziert werden und der daraus errechnete molare Absorptionskoeffizient korreliert sehr gut mit Referenzdaten aus der Literatur. Mit etwas Einarbeitungszeit kann man etwa eine Probe pro Stunde vermessen.

Die Spektroskopie Kammer ist gedacht als eine Ergänzung für Studien am HME Prozess, vor allem zum Auslegen möglicher PAT Methoden. Zusätzlich kann sie für jegliche spektroskopischen Untersuchungen an Thermoplasten (in der Kunststoff und Pharmaindustrie) verwendet werden, da sie eine standardisierte Methode zur spektroskopischen Materialcharakterisierung bietet. Die Experimente können in kürzester Zeit mit minimalen Materialverbrauch durchgeführt werden. Es ist sogar möglich, dieselben Proben mit unterschiedlichen Messmethoden durch Austausch der Sonden zu vermessen.

Table of Content

List of Figures

List of Tables

1 Introduction

In the pharmaceutical industry the continuous manufacturing of pharmaceuticals gains in popularity because of the positive effects on production costs, product waste and flexibility by consistently good or even enhanced product quality. The key to successfully implement continuous manufacturing is process understanding and control. One irreplaceable technique for producing drugs is hot melt extrusion (HME), also a common and well understood production method in plastics industries [1]. It can also improve the solubility of poorly water soluble active pharmaceutical ingredients (APIs) with the help of amorphous solid dispersions [2].

HME starts with the feeding unit operation, which provides a stable material flow (in the simplest case consisting of an API, a matrix carrier and some plasticizers) into the material intake section of a twin-screw extruder. All ingredients of the product except the API are summed up as excipients. The main extrusion unit operation consists of several different zones along the extruder, where the solids mix up and energy is brought in via the warmer barrels and applied shear forces to form a homogeneous melt. Extrusion also acts like a slight low pass filter trying to compensate short-time feeding problems, e.g. by back-mixing. At last the melt is pressed through an extrusion die and further processing steps follow. To guarantee product quality, in-line process monitoring tools are needed in the die section of the extruder.

Process analytical technology (PAT) is used to monitor and control critical quality attributes, like stable API content with several in-line measurement methods. Common methods are near-infrared (NIR), Raman and UV/VIS spectroscopy. This PAT tools must be calibrated to the actual process conditions. The reference data sets are usually measured inline at the investigated extruder. Because every extrusion process consumes a high amount of material, a lot of effort in material costs, time and process equipment is needed to get accurate data.

To give one example: a small twin screw extruder (e.g. 10 mm with 50 g/h) should run for at least 5 to 10 mean residence times (before stable conditions can be

assumed) and then a stable signal should be recorded for several mean residence times meaning that one typically needs 10-20 mean RTDs for the generation of one data set. Usually for model building a number higher than five is suggested for different concentration levels. Thus, one can sum up to an operation time of 50 to 100 mean RTDs. In case of cleaning, which is usually suggested between different concentration levels, cleaning hours go on top for the generation of a reference set. These runs sum up to significant costs, especially given the expense of recent novel APIs.

The aim of this work is to design a tool that allows the simplified acquisition of reference data sets on polymer melts containing API. The tool should be used to analyze small material samples (<10 g) at elevated temperatures (up to 250°C) with the possibility to mount process sensors which are later used in the extruder. The process sensors are usually mounted in equipment specific ports, resulting in unique positions in terms probe distance in almost every application. The penetration depth of the subjected light beam is crucial for a successful measurement. This parameter was not accessible as only fixed designs for inline sensors existed. The vacuum compression molding (VCM) tool, also described in the work of Treffer D. [3] and commercialized by MeltPrep GmbH, will form the basis of the spectroscopy chamber. With this technology, it should be possible to reach the high process temperatures, eliminate the occurrence of disturbing bubbles in the melt and be compatible to industry standard spectroscopy probes mounts with the benefit of adjustable distances.

2 Fundamentals of Optical Spectroscopy

Optical Spectroscopy is the interaction of light with matter (in case of HME with the polymer melt). In this particular field not only, the visible radiation (VIS) is referred, but also ultraviolet (UV) and near infrared (NIR). In this thesis two basic setups for spectroscopy, transmittance and reflectance, are used. In transmittance mode the amount of light **passing through** a material and in reflectance mode the amount of light getting **reflected from** the material is measured. Therefore, the former method is for translucent substances, the latter for opaque and powdery ones.

2.1 Beer–Lambert Law

The absorption of a light beam by a medium at a specific wavelength λ can be characterized by the absorbance $A(\lambda)$ or the transmittance $T(\lambda)$ as stated in Eq. (1). I_λ^0 is the light intensity entering and I_λ the light intensity leaving the absorbing medium.

$$A(\lambda) = -\log T(\lambda) = \log \frac{I_\lambda^0}{I_\lambda} \tag{1}$$

According to Beer's law (Eq. (2)), the absorbance is usually proportional to the molar absorption coefficient $\varepsilon(\lambda)$ (usually in $L \cdot mol^{-1} \cdot cm^{-1}$), the concentration of the absorbing substance c (in $mol*L^{-1}$) and the absorption path length l (in cm).

$$A(\lambda) = -\log T(\lambda) = \log \frac{I_\lambda^0}{I_\lambda} = \varepsilon(\lambda) * l * c \tag{2}$$

For analytical applications in many cases the absorption by a specific substance in a solvent, and not by the solution itself is from importance (e.g. determine the concentration of a substance in a solvent). In this case I_λ^0 is not the light intensity entering the solution, but the light intensity leaving the pure solvent (called reference medium or blank) determined in separate performed measurement [4]. In this way the absorption of the solvent or any secondary substance is filtered out.

2.2 UV/VIS Spectroscopy

In UV/Vis spectroscopy the absorption of light is measured in the wavelength range from about 200 to 700-800 nm. Usually, the light is emitted by a deuterium lamp (for analysis in the deep UV), tungsten lamp (for VIS and NIR) or a xenon flash lamp (for analysis in the UV and visible regions).

The absorption of a molecule could be described by the transition from a lower to a higher electronic state induced by the absorbed photon. There are three types of electrons in a molecule, forming molecular orbitals: σ, π and n electrons. A σ-bond is a single bond as it occurs in methane (C-H) or ethane (C-C). A π-bond usually appears in combination with a σ-bond in form of a double (one σ and one π) or a triple (one σ and two π) bond as it occurs in ethylene or acetylene. Nonbonding n electrons appear for example on the oxygen atom of water or on hydrogen fluoride.

There are five transition that may occur ordered according to their energy:

$$n \rightarrow \pi^* < \pi \rightarrow \pi^* < n \rightarrow \sigma^* < \sigma \rightarrow \pi^* < \sigma \rightarrow \sigma^*$$

whereas the * indicates the corresponding antibonding orbital.

The lower the energy of the transition, the higher the wavelength of the absorbed photon. Most of the absorption in the UV range occurs due to n and π-electron transitions, as the promotion of a σ electron requires too much energy and appears only in the far UV [4]. The strongest transitions are generally between the HOMO (highest occupied molecular orbital) and the LUMO (lowest unoccupied molecular orbital) involving $\pi \rightarrow \pi^*$ in the visible (Vis) regime.

With UV/Vis it is possible to measure color changes of polymers during extrusion. Since many hormones and APIs are UV active, this spectroscopy method works well for many applications in the pharmaceutical field [5] [6].

2.3 Near-Infrared (NIR) Spectroscopy

IR spectroscopy uses the fact that the bonds in a molecule are excited to higher vibrational states when they absorb electromagnetic radiation with an appropriate

frequency. The characteristic frequency of a bond in a heteronuclear diatomic molecule usually increases with the order of the bond and decreases with the reduced mass of the atoms [5]. The NIR wavelength ranges from about 800 to 2500 nm and is basically too low for most fundamental frequencies arising from the molecular skeleton (C-C, C=C, etc.) or from functional groups containing heavy atoms (C-Cl, C-N, etc.) and their weak overtones. Therefore, the NIR range covers principally overtones and combinations of lower energy fundamental molecular vibrations. Most organic compounds contain at least one X-H bond vibration which have luckily a very high sensitivity to near neighbors in the molecular structure [7]. For this reason, NIR spectroscopy is well suited for detecting moisture (O-H group), amines (N-H) and hydrocarbons with characteristic X-H groups.

2.4 Raman Spectroscopy

Raman spectroscopy also involves transitions between different molecular vibrational states. But in contrast to IR spectroscopy the Raman effect is the non-elastic scattering of photons. This can be described by absorption and instantaneous emission of a photon, involving a virtual exited state. Normally, the molecules are excited by a laser generating a defined excitation frequency (ν_{ex}). The emitted photons differ from the excitation frequency by $-\nu_i$ (Stokes scattering) or by $+\nu_i$ (anti-Stokes scattering) and are measured by the Raman spectrometer. Stokes scattering occurs if the molecule gains energy from the absorption, anti-Stokes scattering if the molecule is already in a higher vibrational state during the absorption. Because the lowest vibrational mode of molecules is usually occupied and only exited to higher states by temperature, the strength of anti-Stokes scattering increases with temperature of the material. Both scattering effects increase if the light falls within a molecular absorption band (called resonance Raman scattering) [5]. The Raman shift is independent from the excitation frequency and is well suited to identify molecules because vibrational frequencies are like a fingerprint and specific to the chemical bonds of a molecule.

3 State of the Art

This chapter should show up actual calibration methods, technical and mathematical background to the process probes and some effects that could have an impact on the spectra.

3.1 Existing Calibration Methods

Studies on in-line spectroscopy methods are usually done directly in an HME process, ideally on a little extruder with small batch sizes due to the commonly high material costs in pharma applications. Some typically feeding rates range from 0.1 to 1 kg/h, with subject to change [1], [8], [9], but typically at least one order of magnitude below the actual desired rates of the process. To build a chemo-metric model, spectra of varied known input variables (like API content, process temperature, etc.) have to be recorded. The chemo-metric model uses these observables of known variables to predict the unknown variables online in a running process. This calibration procedure consumes much time and respectively a high amount of material. One manufacturer of offline transmission cells for fluids circulating through a chamber is the company Specac Ltd (www.specac.com).

Fig. 3-1: From left to right, Omni-Cell System, High Pressure Liquid Cell and Variable Pathlength Cell from Specac Ltd **[10]**.

In Fig. 3-1 some products are shown, including the high-pressure cell (up to 5000 psi) and the variable pathlength cell (for changing probe distance during transmission measurement). They provide different window materials to suit various spectroscopy methods and a 3" x 2" mounting plate [10].

These cells suffer from several disadvantages. First the mounting is not directly compatible with industry standard process probes with a Dynisco head: 1/2"-20 UNF-2B [11]. Extruder channels are already equipped with these standard ports because this is also the typical fitting of pressure probes. Secondly, to get close to process conditions the probes should not be separated from the melt by an additional window.

Furthermore, these cells are optimized for measurements of liquids in the chemical and petroleum industry and not specially designed for hot melt extrusion. They are incapable of melting polymer powders properly and therefore it is still necessary to install an upstream extruder.

Because of these deficiencies offline calibration might be performed by direct contact of the probe with a piece of cold sample. Obviously, this does not mimic process conditions, because the material is not melted but solid and the probe itself is not fully covered by the sample, especially if the probes' head is not plane but convex because of the probes' lens optics (see Fig. 3-2).

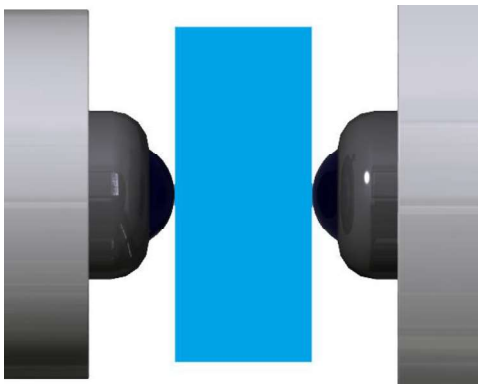

Fig. 3-2: Transmission measurement performed by direct contact of the probe with a piece of cold sample.

3.2 Spectroscopy Methods in HME

There are many spectroscopy methods out there with different pros and cons depending on their application field. This work will concentrate on the prime in-line methods used in pharmaceutical HME processes. According to Hitzer the main optical spectroscopy techniques suitable to detect the crystalline API content are Raman, near-infrared (NIR) and UV/Vis spectroscopy [2]. UV/Vis and NIR are suitable for transmittance and reflectance measurements, whereas Raman is only available in reflectance mode.

3.3 Temperature and Pressure Dependence

According to Wülfert F. there are several process variables such as temperature, pressure and flow turbulence that can affect the measured NIR spectra [12]. They have an influence on the molecular bonds and further on the vibrational modes. This effects especially aqueous materials like ethanol/water/2-propanol mixtures [12] or red and white wines [13].

For upscaling, the measuring conditions should not vary too much from the process conditions, to get representative calibration data. There is little known in literature for pressure and flow dependence of spectroscopy methods.

3.3.1 Pressure

The pressure at the extruder die can reach up to several hundred bars, whereas the pressure in the spectroscopy chamber will only be a few bars (depending on the geometry of the piston [3]). This could lead to two problems: For one thing a possible direct influence on the spectra (see example in Fig. 3-3) and for another thing an impact on the solid state structure and relaxation time [14] of the material.

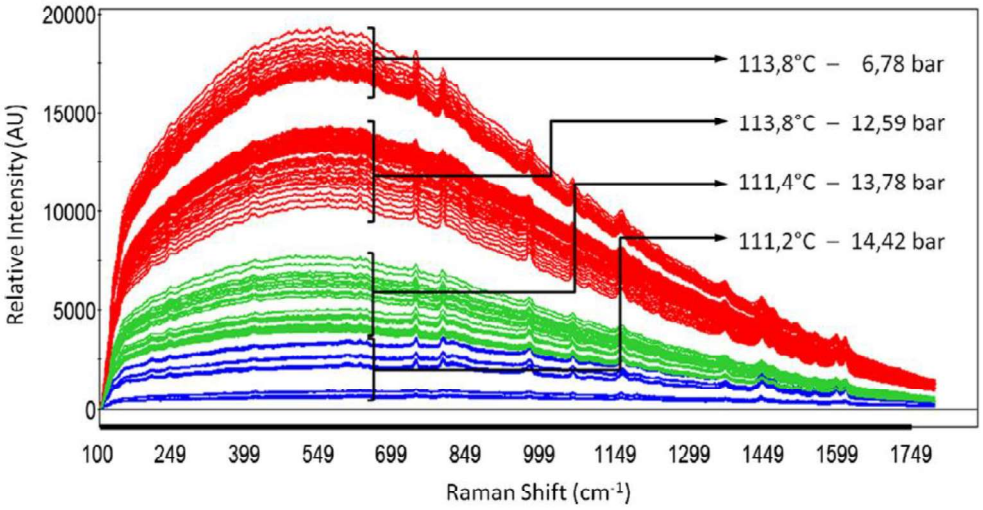

Fig. 3-3: Raman spectra intensity due to pressure change in a pharmaceutical HME process of Celecoxib in a Eudragit® E PO matrix investigated by Saerens **[9]**.

The influence of the pressure on the Raman spectrum is also investigated by Saerens in a pharmaceutical HME process [9]. A higher pressure leads to a decrease in Raman intensity caused by scattering losses due to heterogeneities induced by pressure gradients. Moreover, a pressure induced change of absorption coefficient results in an intensity decrease.

3.3.2 Temperature

Saerens L. investigated the influence of the extrusion temperature on the polymer-drug melt behavior during an HME process of 40% metoprolol tartrate (MPT) and 60% Kollidon® SR. NIR can more than monitoring the API concentration, it is also capable of capturing changes in solid state of the extrudates (the lower temperature was below the melting temperature of MPT) [8]. Therefore, it is important to use the same temperature, or at least a temperature where the solid-state structure of the material appears similar to the process. With the VCM tool as basis it will be possible to adapt the temperature to the required values and so it should not be a limiting parameter.

3.4 Probe Material and Design

The shell of the optical probes is made of TiAl6V4 [15]. Advantages are the low thermal conductivity (a third of stainless steel), the low thermal expansion coefficient (lower than stainless steel and aluminum) and the high mechanical strength under extreme temperatures. Inside the shell are optical fibers carrying the light from the light source to the material. At the end of the probe is a small sapphire window which is transparent for the required spectra. The probes are compatible with the Dynisco thread 1/2"-20 UNF-2B, a standard mount for HME pressure sensors.

3.4.1 Optical Fiber Cable

A waveguide is used to carry the photons from the light source with the help of total inner reflection to the material and vice versa to the detector. Usually, the light beam gets refracted if it passes from one material to another (with different refractive indexes) similar to an eyeglass lens or water appearing to our eye as a distortion. The angle of refraction depends on the angle of incidence according to Snell's law and the refractive indexes of the materials as defined in Eq. (3) & (4) and can be seen in Fig. 3-4.

$$n_i = \frac{velocity\ of\ light\ in\ vacuum}{velocity\ of\ light\ in\ medium} \ldots refractive\ index\ of\ material\ i \tag{3}$$

$$\frac{\sin\theta_1}{\sin\theta_2} = \frac{n_2}{n_1} \ldots Snell's\ law \tag{4}$$

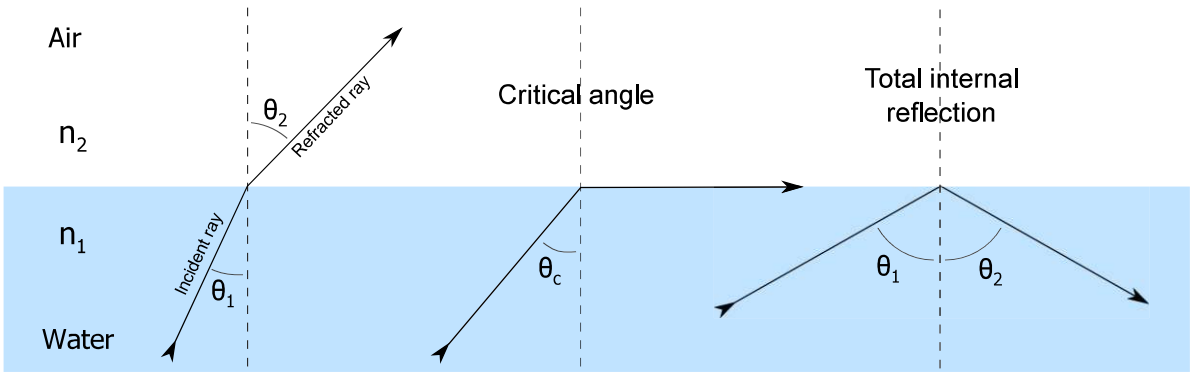

Fig. 3-4: Refraction, critical angle and total internal reflection of light with water and air as example mediums **[16]**.

Total inner reflection can only occur if a light beam hits the border to an optically rarer material with lower refractive index under a shallow angle (water to air, cold air to hot air, etc.). It gets total reflected if the angle of incidence is equal or greater than the critical angle (because $sin(\theta_2) > 1$ is not possible). From this follows the equation of the critical angle, (Eq. (5)). A simple sketch of an optical fiber is shown in Fig. 3-5. Because refraction is also present on the flat entry surface of the fiber, rays outside the acceptance angle θ_{max} are not carried by the waveguide.

$$\theta_C = arcsin\left({}^{n_2}/_{n_1}\right) \dots critical\ angle \tag{5}$$

$$if\ \theta_1 \geq \theta_C\ total\ reflection\ occurs$$

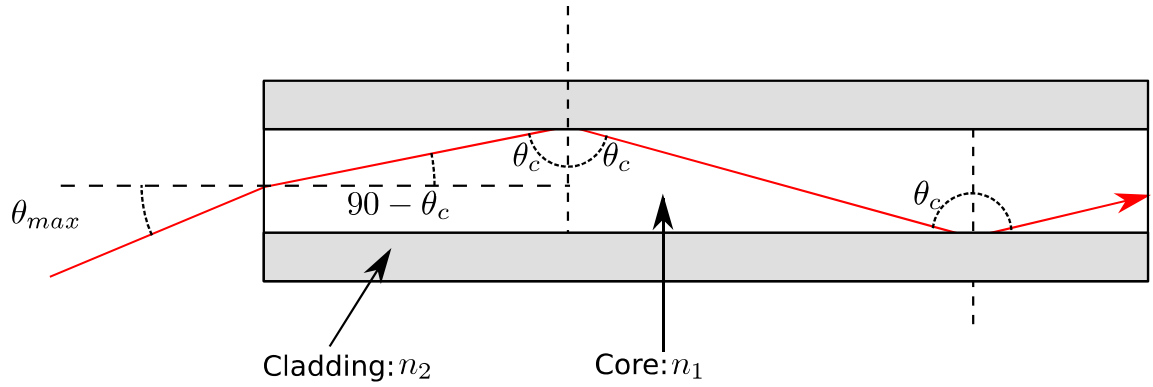

Fig. 3-5: Reflection of light in a waveguide **[17]**.

3.4.2 Reflectance Probes

In the simplest case the probes have a plan sapphire window with an attached optical fibre, see Fig. 3-6. The cable consists of several individual fibers bundled together to form illumination fibres at the outside, arranged in a hexagonal form, and one fiber bundle in the center for detection. The emitted light gets reflected back from the surface of the material and is caught by the inner fiber bundle and guided to the detector. In this way opaque materials can be analyzed. In contrast to conventional reflection probes the ones used in the ColVisTec AG device have a collimator lens at their end. This collimates the illumination beam and focuses the reflected light or in other words increased the numerical aperture.

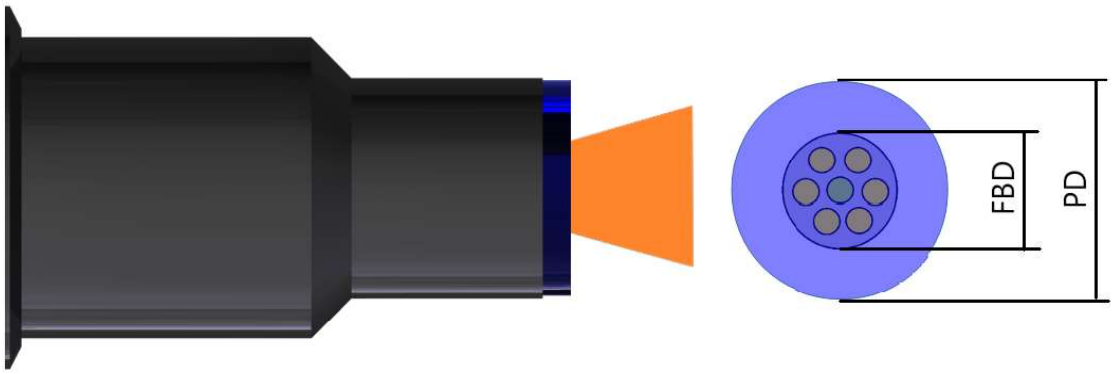

Fig. 3-6: On the left a conventional reflectance probe from the side view with plan sapphire window (and possible light beam) is pictured. On the right the cross-section of the optical fiber bundle(with diameter FBD) laying behind the sapphire window found in reflectance probes (with diameter PD) **[11]** is shown.

3.4.3 Transmission Probes

For transmission two probes are necessary, one for illumination and one for detection (see Fig. 3-7). Both probes have an optical lens to focus the light for increased intensity. Otherwise most of the emitted light cannot reach the opposite probe and is diffused through the main material. In this way translucent materials can be analyzed. This is the reason why radial and axial alignment becomes important.

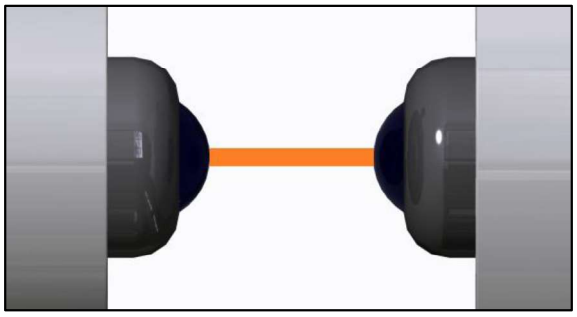

Fig. 3-7: Transmission probes with sapphire lens (possible light beam is shown). 3D probe model is from ColVisTec AG.

The ColVisTec AG UV/Vis probes can be used for reflectance and transmission. For transmission measurements one probe is used as a light source and the other one as the detection probe, using only the center fibers.

3.4.4 Transflectance Probes

There is a special transmission variant called transflectance (e.g. transflectance POLYPRO probe from SOLVIAS AG). In this case one probe acts like a reflectance probe and the other one like a mirror. The light passes the material twice and therefore the intensity decreases, but the setup is simpler, more cost-effective and can be used in processes with varying substance opacity [18].

3.5 Penetration Depth

The penetration depth is an important parameter for inline monitoring of extrusion processes and strongly depends on spectroscopy method and material. According to Wahl embedded API crystals (acting as optical impurities) also affect penetration depth and it has a direct influence on the sample volume approximated by Eq. (6) [1].

$$V_{Sample} = \frac{d^2}{4} * \pi * \lambda + t * d * \int_{R-\lambda}^{R} v(r)dr \tag{6}$$

With d as the diameter of the illuminating spot, λ as the penetration depth, v(r) as the velocity of the material, R the radius of the die section (of the extruder) and t as the integration time [1]. It is hard to measure or calculate the penetration depth accurately and is assumed by Wahl to be 500 µm with NIR spectroscopy in an opaque CaSt-paracetamol melt.

To measure the penetration depth of NIR Clarke performed studies with layers of cellulose papers on a hydrochloride substrate, see Fig. 3-8.

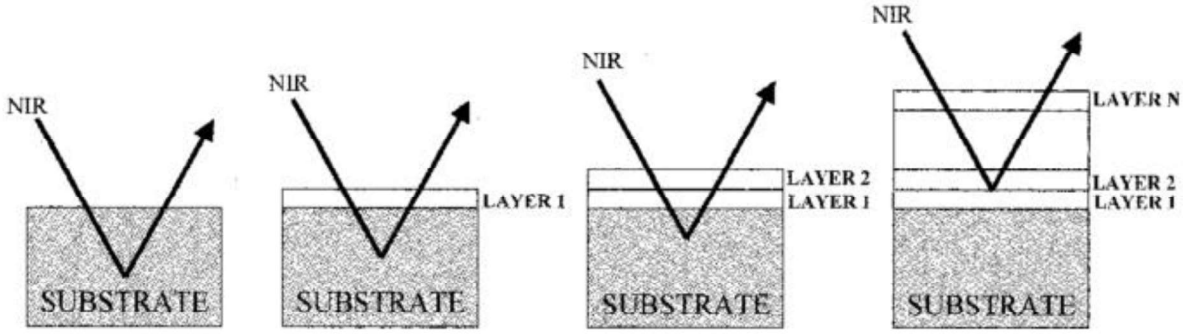

Fig. 3-8: Example how Clarke performed the studies on NIR penetration depth with cellulose layers **[19]**.

This technique only works well for solid materials. Since the distance to a possible substrate material or another light catching probe can be adjusted, the spectroscopy chamber could help measuring the penetration depth for different combinations of materials, temperatures and spectroscopy techniques.

3.6 Flow Boundary Conditions at Processing Sensors

A low penetration depth of the light (like it appears in reflectance mode) means that the gained information is only representative for the material flowing near the sensor. The idealized Hagen-Poiseuille and plug flow like it appears in an extruder die is shown in Fig. 3-9. The flow velocity on the wall (and on the sensor surface) is almost zero and therefore, possible composition fluctuations would appear later in the resulting spectrum.

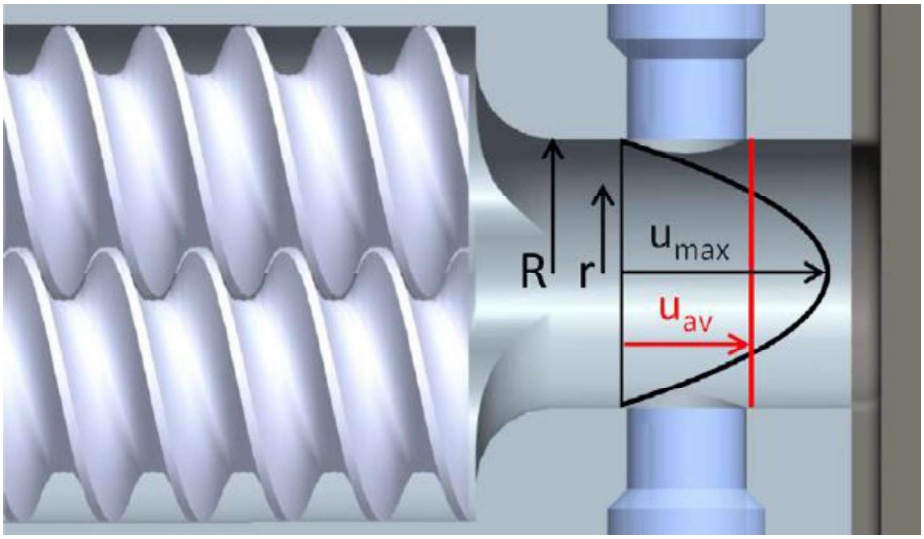

Fig. 3-9: Hagen-Poiseuille flow (u_{max}) and plug flow (u_{av}) in the die section of an extruder. Possible spectroscopy probe positioning is also shown **[1]**.

Furthermore, due to the high shearing rates in an extrusion process the viscosity of the material decreases. The highest shearing rates are in the screw section, but they also appear in the die section of the extruder. A higher slope in the velocity profile also means higher shear rate. Therefore, the shearing rate has his maximum at the wall of the die. So, the real flow velocity profile for shear-thinning non-Newtonian fluids is between the Hagen-Poiseuille profile and plug flow. As a result, there could be an influence by the shear rate on state sensitive spectroscopy methods like Raman (also mentioned in chapter 3.3.1).

3.6.1 Wall Slip

The Newtonian fluid model has simplest boundary conditions, but it can predict the behavior of most important fluids (alcohol, water, air) very well. The viscous stress forces are linear proportional to the local strain rate of the fluid and flow velocities at the wall are assumed as zero [20].

For many other substances including polymer melts this model is very inaccurate. Wall slip occurs and could lead to decreasing product quality due to surface distortion. Ramamurthy studied the behavior of LLDPE, HDPE and HP-LDPE and their difference in behavior. In capillary rheometer experiments he discovered that above a critical shear stress wall slip occurs or to be precise it is recognizable by the onset of surface melt fracture. Within the investigated temperature range (180

– 220°C) the critical stress value is nearly the same for all polymers and ranges from 0.1 to 0.14 MPa and therefore independent of the molecular structure [21]. In Fig. 3-10 this effect can be seen in the example of a Couette flow. The wall slip velocity u_s adds to the static plate and subtracts from the moving plate.

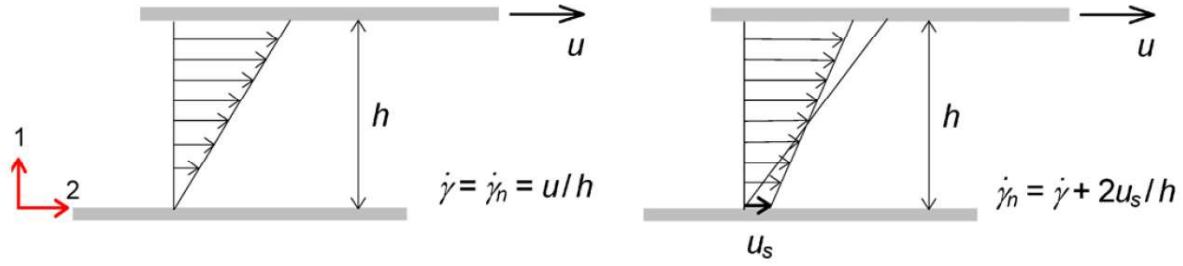

Fig. 3-10: Couette flow profile under no-slip (left) and slip conditions (right) **[20]**.

3.7 Need for an Offline Tool

PAT is an important field in the pharmaceutical industry to guarantee product quality, especially in terms of API content and molecular state. But besides that, degradation, ratio of excipients, temperature, pressure and so on have an influence on the resulting spectrum. Different spectroscopy methods have varying qualities and must be chosen according to monitoring requirements.

Currently in-line tests are the only option to obtain reliable insights if the chosen spectroscopy method, e.g. UV/Vis, is applicable for the desired PAT task. A process engineer would need to monitor the extrusion process of an UV active API with UV/Vis spectroscopy probes. Regrettably, one has not considered or simply not known that the polymer matrix blocks completely in the absorbing UV range of the API. After the first extrusion experiment with 1kg material and several hours of preparation the resulting spectrum is unusable or affected by intense signal noise.

That could have been prevented by analyzing a small dose (under 10 g) in an offline tool, the spectroscopy chamber. As a side benefit one can visualize the melting range, solubility of the API, behavior at different temperatures, transparency (especially at different distances), degradation and a lot more in just one experiment. Being compatible to the original process probes one gets a perfect insight how the polymer interacts with the applied light with minimum time and effort. Afterwards the sample can be taken out and further analyzing is possible.

4 Design of the Spectroscopy Chamber

The aim of this master thesis is to invent a new and standardized way of developing and analyzing API formulations used in HME. The goal is to design a small chamber for testing different API-polymer combinations and spectroscopy methods, therefore the thesis involved a basic constructive part from scratch. The starting material (a polymer granule or powder mixture as used in HME) should be melted in a closed system between two spectroscopy probes to investigate the behavior of the resulting spectrum. To guarantee a straightforward handling and easy cleaning at the hands of unexperienced users, the focus of the main construction lays on the so-called KISS[1] principle (also mentioned in the work of Kreutz et al. [22]). The biggest challenge was to implement the regulation of the probe distance during the measurement. Fortunately, the VCM tool follows the same structural principle and it is therefore eminently suited to be the basis of the spectroscopy chamber [3].

4.1 Development Requirements

The idea is to design a dismountable chamber in which a polymer-API combination is filled in (like the VCM Tool [3]) and gets molten between two spectroscopy probes to provide similar conditions to PAT analysis in HME. It should be variable in temperature and probe distance during measurement and be compatible with industry standard process probes.

Despite of that the melting process should inhibit the occurrence of bubbles and the chamber should be easy to handle and clean (without further tools). By using the VCM technology as basis for the spectroscopy chamber a few requirements are checked. The temperature variability is ensured by using an adjustable hotplate and cleaning effort is kept to a minimum by using separation foils (patented by MeltPrep GmbH) at the walls of the chamber. By applying pressure via a vacuum

[1] Keep it simple [and] stupid

driven piston, the occurrence of bubbles will be prevented because remaining air in the powder is sucked out before melting.

Most important design requirements to the chamber are:

- Measurements starting from powders
- Temperature variability during measurement (room temperature – 250°C)
- Probe distance variability during measurement (0-10 mm)
- Compatible with industry standard process probes (Dynisco 1/2" UNF)
- Easy cleaning.
- Operation without tools (wrench etc.)

4.2 Concept

The first idea was to take the VCM tool as it is and try to enhance its capabilities step by step. The fact that the moving piston of the VCM tool adjusts to different filling heights could also be adapted for the distance adjustment. Placing the probe socket into the top and the bottom of the tool offers the first basic axial probe positioning concept open for further improvements.

4.2.1 Axial Design

The axial design consists of a bore (containing the material) with axially placed transmission probes. To variate the probe distance, it is necessary to bring material in and out of the chamber without opening the device. This could be accomplished by a bore containing a small piston that will be shifted from the outside, also seen in Fig. 4-1. The out and inflowing melt is compensated by the vacuum driven piston (containing one probe) and therefore the probe distance changes.

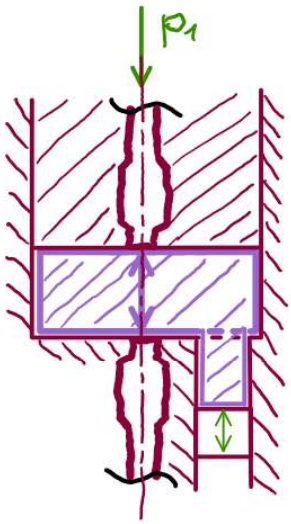

Fig. 4-1: First axial concept of the spectroscopy chamber.

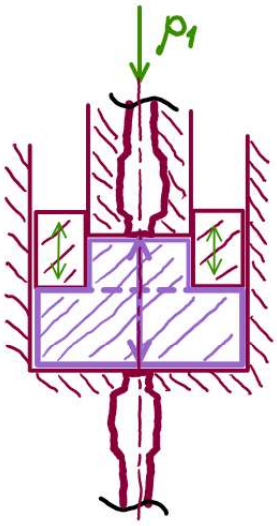

Fig. 4-2: Displacer shell concept.

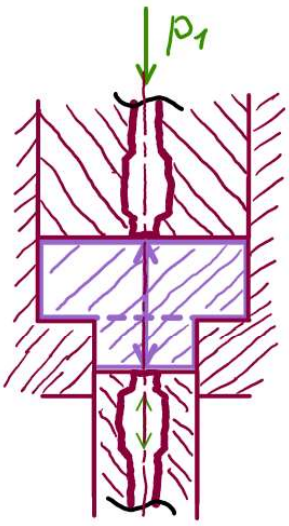

Fig. 4-3: Final concept.

Theoretically it would be easier to install a small drain plug to release melt and lower the volume, but this would deprive the chamber of the possibility to raise the distance and only distance lowering is possible

By improving the axial concept, the idea of a bushing that wraps around the piston and variates the shape of the chamber arose (see Fig. 4-2). It offers a simpler chamber geometry and a compact design. The drawbacks are the tolerance addition in case of the two combined guides and a challenging separation foil and sealing positioning. This leads to the final concept where the shell is substituted by a further piston (Fig. 4-3). If the diameters of the oppositely placed pistons are different they displace a different amount of volume per distance. This results in an inevitable change of the space between the probes.

4.2.2 Radial Design

Apart from that there was the idea of a radial probe position concept providing the possibility to use more than two probes and compare the spectra of different spectroscopy techniques in one pass (see Fig. 4-4). The difference to the axial concept (Fig. 4-3 without the lower piston) is that the probes are placed radially around the chamber. The probes can be moved back and forth and the upper piston will compensate the change in chamber volume. This concept will miss the purpose of the KISS principle by increasing geometry intricacy and cleaning effort.

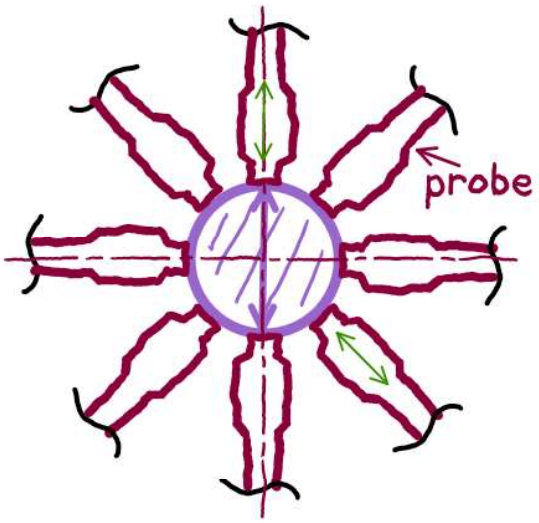

Fig. 4-4: Radial concept.

4.3 Prototype

The axial design concept as illustrated has been chosen for the construction of the prototype. In Fig. 4-5 the sectional view of the first prototype is shown. The main parts of the construction are the body itself and the pistons with the probe mounting holes. The body is made from a big aluminum cylinder to ensure that the pistons guides can be manufactured on a lathe without rechucking (repositioning) to guarantee axial alignment. The guiding part and the mounting holes of the pistons are also manufactured on a lathe (turning machine) in one step. The lid and the socket should hold the pistons in place and seal the chamber and the lid applies pressure on the smaller piston. Between the body and the pistons PTFE foils are placed to prevent the material being in contact with the metal. That is the reason why the pistons and the lid and the socket are separated parts. In this way it is possible to have a view on the pistons when threading them in. To allow distance regulation the adjusting nut pushes the socket forward or backwards. The bolts prevent the probes from twisting.

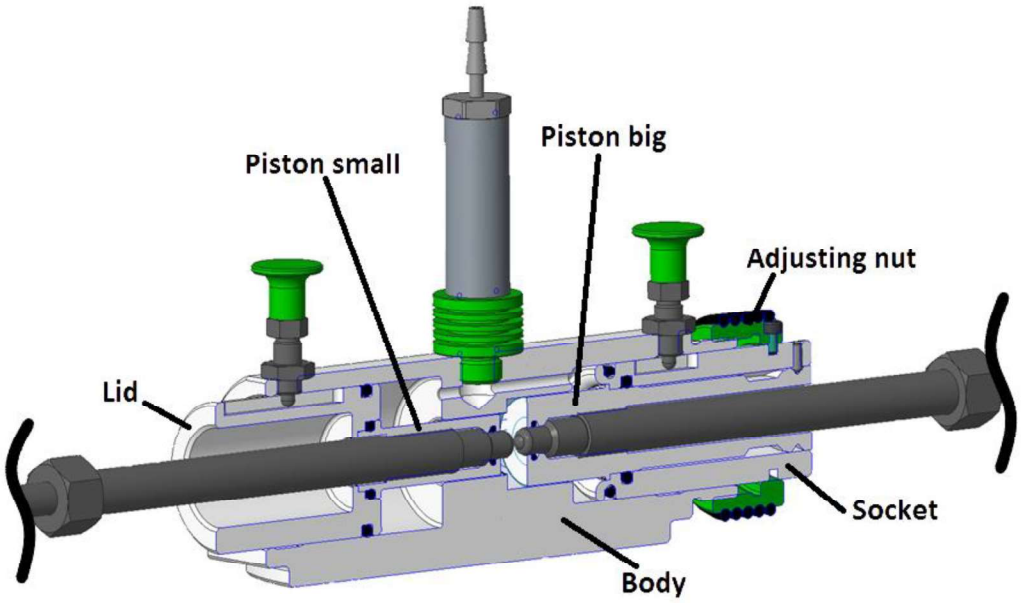

Fig. 4-5: First prototype of the spectroscopy tool. Sectional view with peek (polyether ether ketone) elements (green), probes (dark grey) and the aluminum chamber with components (light grey).

The sample volume is situated between the two probes. When vacuum is applied on the chamber (at room temperature) air molecules between the filled in granulate are removed and the ambient pressure acting on the sensor lids compacts the granules. To prevent air leakage the pistons and bushings are sealed with O-Rings made of FKM (fluoroelastomer) due to the high temperature resistance.

4.3.1 Probe Distance Adjustment

The probe distance adjusts by the fact that the different piston diameters displace a different amount of volume per distance. The sample volume stays constant (except for thermal expansion or different filling heights) the change in distance is also constant. In Fig. 4-6 this effect is illustrated with three different probe distances for a give sample volume.

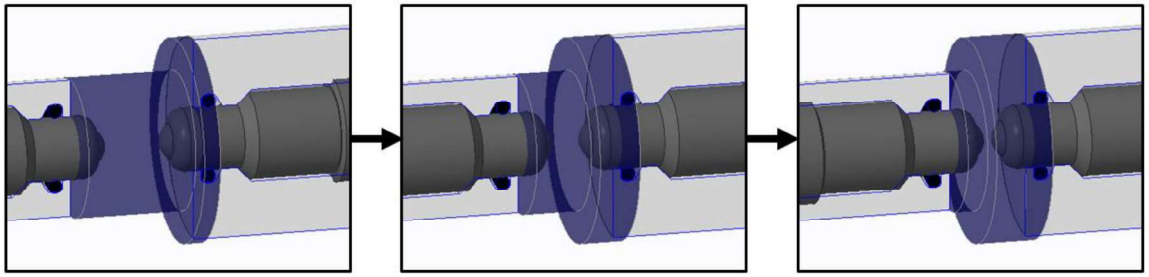

Fig. 4-6: Distance adjustment from high (left) to low (right). The molten sample is pictured in between the two transmission probes.

The probe distance follows a linear function depending on the two associated diameters and the travel range of one piston (expressed by the thread pitch times revolution of the adjusting nut), see Eq. (7) and Fig. 4-7.

$$\Delta h(U) = U * P * \left(\frac{D^2}{d^2} - 1\right) \tag{7}$$

$$with\ D = 25\ mm, d = 17\ mm, P = 1.5\ mm$$

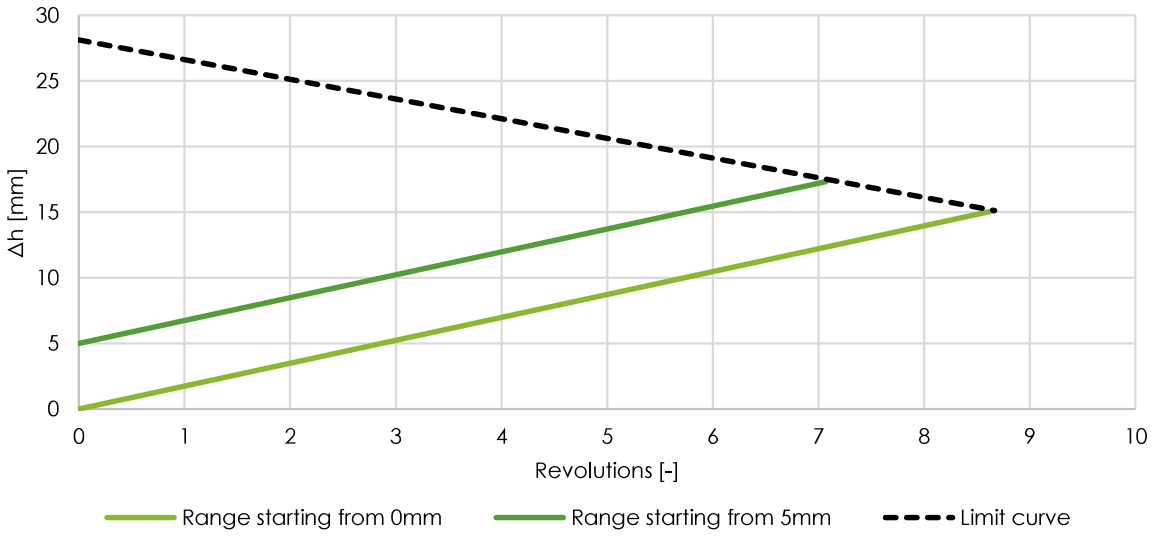

Fig. 4-7: Probe distance versus revolutions with a M45 x 1.5 thread on the adjusting nut.

The maximum range is from 0 to 15 mm (ColVisTec transmission probes, powdery starting material and correct filling implied). A higher filling volume lowers the range but raises the maximum distance. The theoretical maximum probe distance of melts is 28 mm, but this value is hard to reach as the bulk density of the compacted starting material (powder or granule) is lower than the density of the

formed melt as a rule of thumb ½ of the solid density. If higher distances are required one could consider loading solid discs with 25 mm in diameter as starting material.

4.3.2 Dynisco Thread and Sealing

The probes mounting holes are defined by the Dynsico thread standard 1/2”-20 UNF-2B initially used for pressure sensing probes in the extruder die as seen in Fig. 4-8. Since no special tool kit for manufacturing of the mounting holes was available there are some challenging parts. The axial alignment of the holes and the 45° cone, the short thread run-out before the cone and the O-ring placement (as seen in Fig. 4-9) in the small 8 mm bore where the probe lens comes out.

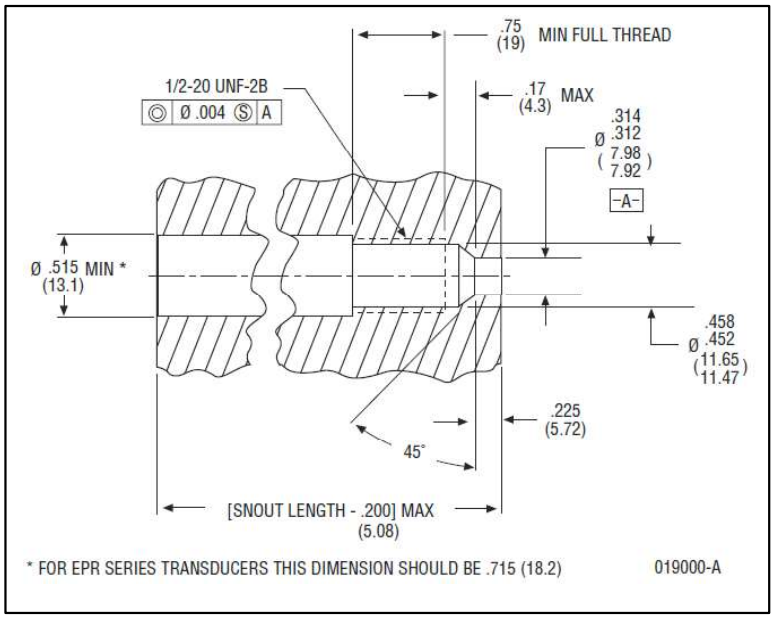

Fig. 4-8: Mounting hole details for the standard Dynisco thread **[23]**.

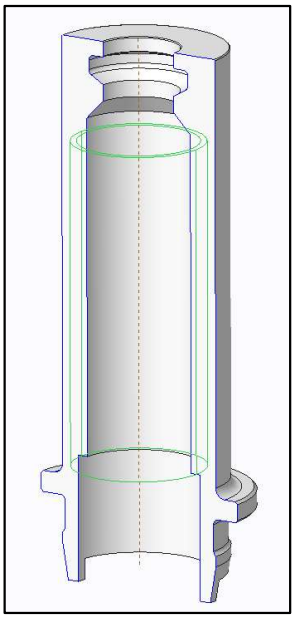

Fig. 4-9: The small 17mm piston with Dynisco hole and additional O-ring mounting.

The O-ring is important to prevent melt penetrating into the thread and keep cleaning simple. Usually, the cone alone acts like a metallic surface seal, but this requires high forces and would be to the detriment of handling and cleaning. For removing the O-ring a small tool is needed, but it helps to put the whole piston into acetone until everything is clean and the O-ring swells up and can be removed very easily.

4.4 Design Verification

This chapter covers the first tries with the spectroscopy chamber and basic experiments. The axial alignment stability should show the stiffness against forces applied on the probes and the temperature curve gives an idea about the magnitude of the heat up time.

The first cold test was done at room temperature with around 6 cm^3 foam material inside to prevent the pistons from hurtling into each other when applying vacuum. The whole setup can be seen in Fig. 4-10. At the beginning the separation foils at the walls must be inserted into the chamber (see Fig. 4-11). Next step is to install the small piston (shown in Fig. 4-12), which should already be mounted with the probe and the lid. Afterwards all the circular separation foils and the polymer must be inserted. Last step is to put in the big piston (also mounted with the probe, the adjusting nut and the socket as seen in Fig. 4-13). During the assembling, the socket should hang loosely on the shaft of the probe to allow a good view to the chamber when inserting the piston.

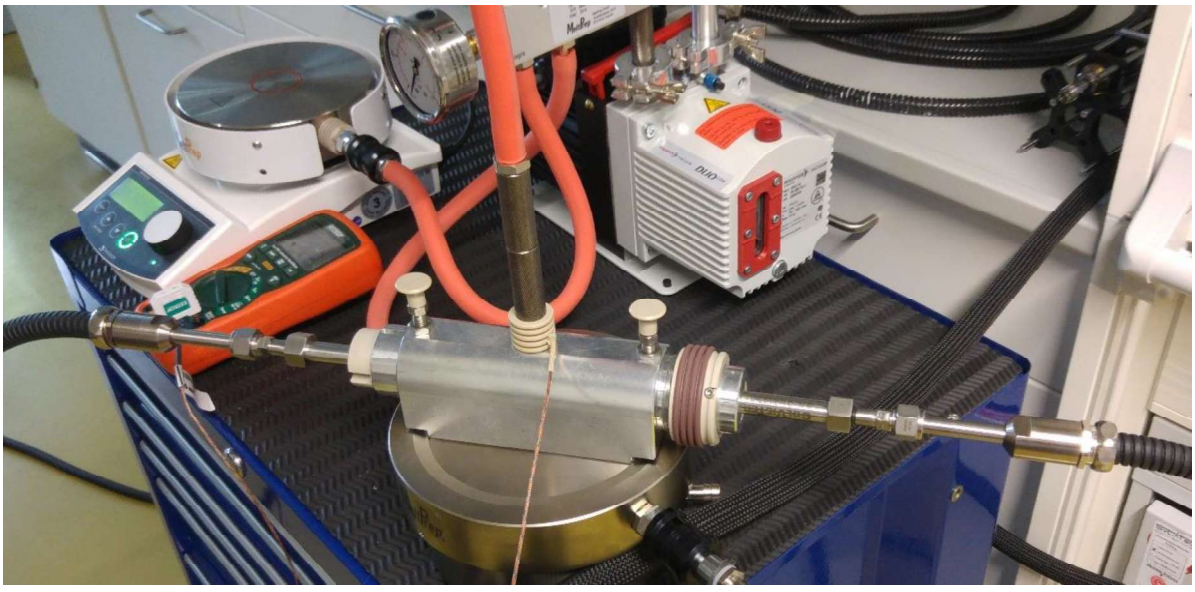

Fig. 4-10: Complete setup with the spectroscopy chamber and the VCM Essentials.

Fig. 4-11: Insert separation foils.

Fig. 4-12: Small piston with probe.

Fig. 4-13: Big piston with probe.

4.4.1 Axial Alignment

For accurate transmission measurement the probes need proper axial alignment. Precise manufacturing should prevent the radial and angular displacement. Since the probes are very long and have a long free-hanging optical fiber cable on their end there is a not negligible force on them slightly bending the probes downwards (acting as external initiated angular displacement). This results in a lower intensity of the spectra.

According to Andreas Berghaus, Director of Engineering & Technology at ColVisTec AG, the intensity decrease should be lower than 1% and optimally under 0,1%. The axial alignment stability was tested by raising each probe separately until the chamber lifted off and setting the resulting intensity in ratio with the intensity of the initial position, as seen in Fig. 4-14. The reference material was air and there was no vacuum applied (and therefore no vacuum driven stability force).

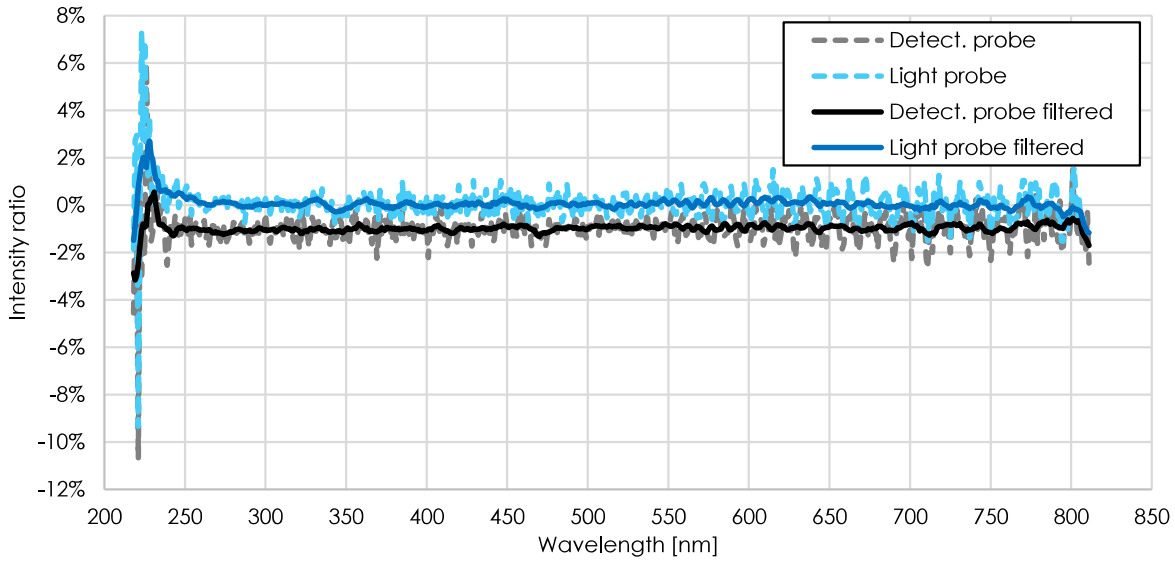

Fig. 4-14: Deviation from initial position by raising detection probe or light probe with 10mm probe distance in percent (ET: 10 ms, NoF: 2). The filtered signal is smoothed by Savitzky-Golay-Filter with a window size of 10 and a polynomial order of 2.

The high scattering in the lower wavelengths could appear due to higher refraction and noise (explained later in the experimental part) in these regions. Above 250 nm the drift is around 1%. The higher scattering in the higher wavelengths can also be explained by the lower light intensity of the lamp in these regions.

4.4.2 Temperature Curve

The chamber is heated from the bottom by conduction using the hot plate of the VCM Essentials. The plate is preheated to the desired temperature (a few degrees more to get a temperature gradient) for faster heat up times. In Fig. 4-15 the temperature curve from a heat up to 130°C is shown. The hot plate temperature was set to 133°C.

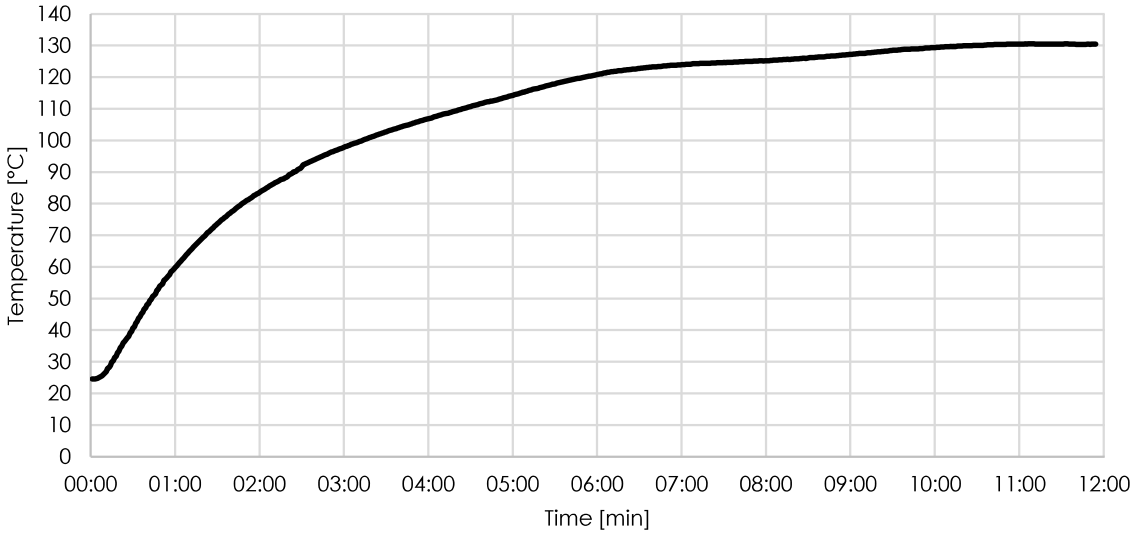

Fig. 4-15: Temperature curve from a heat up of 5g Eudragit® E PO. The target temperature was 130°C and the hot plate was set to 133°C.

The chamber needed about 11 minutes to heat up from 25 to 130°C. Covering the chamber with isolating material does not affect the heat up time at all, but it lowers the needed temperature gradient a bit (normally the hot plate should been set up 3 to 5 degrees over the desired temperature).

5 Materials and Methods

This chapter should show up the materials and spectroscopic tools used in the subsequent experiments. Furthermore, the main parameters set in the respective spectrometer are listed.

5.1 Materials

Various polymers are used in pharmaceutical industries having the potential of being an appropriate test material. In this thesis mainly used substances were EVA28 (pure and with API) and Eudragit® E.

5.1.1 EVA28 [24937-78-8]

EVA28, primary used as membranes and backings in laminated transdermal drug delivery systems, is an ethylene vinyl acetate copolymer (EVA) with a vinyl acetate content of 28%. In Fig. 5-1 the principal structure of EVA can be seen, with subscript "m" indicating the vinyl acetate and subscript "n" indicating the ethylene group. As seen in Fig. 5-2, it is a translucent white waxy solid available in pellet or powder form [24].

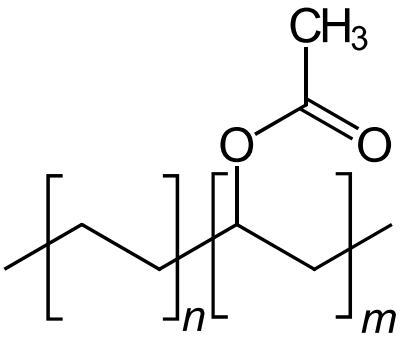

Fig. 5-1: Structure of ethylene vinyl acetate copolymer [25].

Fig. 5-2: EVA28 sample from a spectroscopy chamber experiment.

EVA28 is investigated in pure form and in combination with the API Estriol to verify the detection of API in the spectroscopy chamber. More about that in chapter 0.

5.1.2 Eudragit® E [24938-16-7]

Eudragit® polymers, a product family from the company Evonik Industries, belong to the polymethylmethacrylates and are primarily used as film-coating agents in oral capsule and tablet formulations. Eudragit® E in particular is chemically called Poly(butyl methacrylate, (2-dimethylaminoethyl) methacrylate, methyl methacrylate) and is a translucent glassy solid available in granule (E100) and powder (E PO) form [24]. Experiments with Eudragit® E were only carried out in pure form.

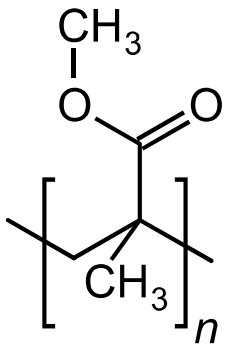

Fig. 5-3: Structure of polymethyl methacrylate [26].

Fig. 5-4: Eudragit® E100 sample from a spectroscopy chamber experiment.

5.1.3 Estriol (E_3) in EVA28 [50-27-1]

Estriol is the main estrogen in pregnancy and is primarily converted from estrone (E_1) and estradiol (E_2) in the liver or synthesized during pregnancy in the fetal placenta. In medicine E_3 can be used as an safer alternative for postmenopausal women compared to traditional hormone therapies with estrone and estradiol [27]. The chemical structure can be seen in Fig. 5-5. It differs from estradiol only by an additional OH bond.

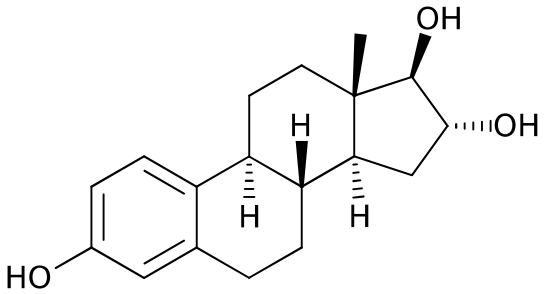

Fig. 5-5: Structure of estriol [28].

E_3 embedded in an EVA28 matrix was used to test the capability of detecting API in the spectroscopy chamber. Extruded EVA28 with 10% estriol content was used for a dilution series with 5%, 2.5%, 1%, 0.5%, 0.1%, 0.01% and 0.001% API content. Afterwards the mixtures were cryomilled for better homogenization. When handling estriol all safety precautions have been observed and only polymer powders with embedded API (not the pure substance) were used. At the end of the experiments the remaining samples were analyzed in the HPLC to get the exact API content. The results can be seen in Table 5-1.

Table 5-1: Target drug loading vs. the corresponding actual drug loading.

Actual E_3 loading [%]	Target E_3 loading [%]
0.005	0.001
0.170	0.100
0.61	0.5
0.82	1.0
2.21	2.5
4.07	5.0
8.48	10.0

5.2 Methods

Since the spectroscopy chamber is adapted to fit process sensors with a specific port it was not possible (and not the intention) to use an off-the-shelf spectrometer from the lab. The majority of the experiments were carried out with the ColVisTec UV/Vis spectrometer bundled with two RPMPs (reflection polymer melt probe).

The Sentronic SentroPAT Analyzer bundled with one reflectance probe was used for NIR reflectance measurements and, with small modifications and limitations, also for transmission measurements.

For Raman experiments the i-Raman® Plus spectrometer in combination with a customized process probe from ColVisTec was used.

5.2.1 ColVisTec InSpectro X

The ColVisTec InSpectro X in combination with two RPMPs (reflection polymer melt probe) was used for UV/Vis measurements. It was designed for continuous in-line process monitoring with a resolution of 1 nm in the wavelength range of 220 – 820 nm, give or take depending on the individual machine (the experiments in this thesis were carried out from 218 to 811 nm). The device, pictured in Fig. 5-6, is an entire PC with a Touchscreen, USB ports, SMA905 glass fiber ports, a built-in spectrometer and a xenon light source. It is preloaded with EquiColor 1.4.0 software, based on Microsoft® Windows 7 operating system [29].

Fig. 5-6: ColVisTec InSpectro X with plugged keyboard and mouse.

A xenon flash lamp produces light in the desired wavelength range. The signal is transferred over glass fiber cables to a RPMP, pictured in Fig. 5-7. To measure in reflectance mode the inner and outer fibers of one probe are connected to the spectrometer, one for illumination and the other one for the detection of the

reflected light. For transmission mode it is necessary to use two probes, but only with the inner fibers of each connected to the InSpectro X. More information on this topic can be found in chapter 0 and 0. The detected light is then measured by the spectrometer.

Fig. 5-7: One RPMP with pulled on lid from the spectroscopy chamber. On the left the smaller piston is shown where the probe fits in. Although it is a reflection probe it has a collimator lens to be also prepared for transmission measurements.

Parallel to the measurement line the signal of the xenon flash lamp is transferred by a so-called light-compensation fiber (LC) directly to the detector. This is necessary to compensate short- and long-term light intensity fluctuations. The settings used for the experiments are shown in Table 5-2.

Table 5-2: Configuration of the ColVisTec InSpectro X.

	Transmission
Averaged exposures per spectrum	5
Resolution	1 nm
Range	218 – 811 nm

5.2.1.1 Optimization and Calibration procedure

The spectrometer should be adjusted and calibrated for every measurement series or when the probes are disconnected. This is done with air as a reference medium at a certain probe distance (in case of transmission measurements) or with a white standard (in case of reflectance measurements). The exposure time (ET) and the

number of lamp flashes per exposure (NoF) change depending on the experiment. Unless otherwise specified the probe distance for calibration and measurement is 6.2 mm as this is the standard probe distance in Leistritz extruders.

5.2.1.2 Optimize Probe procedure

The CCD sensor measures the light intensity for every wavelength as so-called counts. The resolution is 16 bit and therefore a maximum of 65,535 counts is possible. Depending on the material the light reaching the sensor has to be adjusted to prevent the sensor from oversaturation. This is done by adjusting the exposure time (how long the sensor is illuminated) and the number of lamp flashes per exposure in the "Optimize Probe" screen of the EquiColor software. Very translucent materials or smaller probe distances need a shorter exposure time than more opaque materials or bigger probe distances. The goal is that the maximum intensity in calibration lays between 50,000 and 55,000 counts to have a safety margin for the online run.

5.2.1.3 Calibration

The detected signal is always a combination of the light spectrum of the xenon flash lamp, the absorption of the signal path (glass fibers and the lens) and of the analyzed material. As a result, the spectrum has to be referred to a known and reasonable reference spectrum. For API detection this is usually the pure polymer matrix to see only API related changes in the spectrum. In this thesis air is used as the reference for transmission mode since it has nearly no absorption and therefore the result is the clean spectrum of the analyzed material. For reflectance mode a white standard is used as a reference. Furthermore, a black standard is needed to correct the background noise of the sensor.

The reference and the black standard is set in the calibration procedure of the EquiColor software before the actual measurement. It records a spectrum from the selected reference material (pure polymer, air or white standard) and a dark spectrum by covering the input channel to prevent light from reaching the sensor.

5.2.1.4 Calculation of the spectrum

The CCD sensor records the signal from the probe I_{probe_i} and from the light-compensation channel I_{LC_i} (also called reference channel, not to be confused with the spectrum from the reference material) simultaneously. Subscript i stands for the corresponding reference material, sample material or dark standard. The corrected signal calculates according to Eq. (8). For better illustration possible curves of the probe and the LC signal for the reference (air) and EVA28 can be seen in Fig. 5-8.

$$I_{corr\_i} = \frac{I_{probe\_i}}{I_{LC\_i}} \tag{8}$$

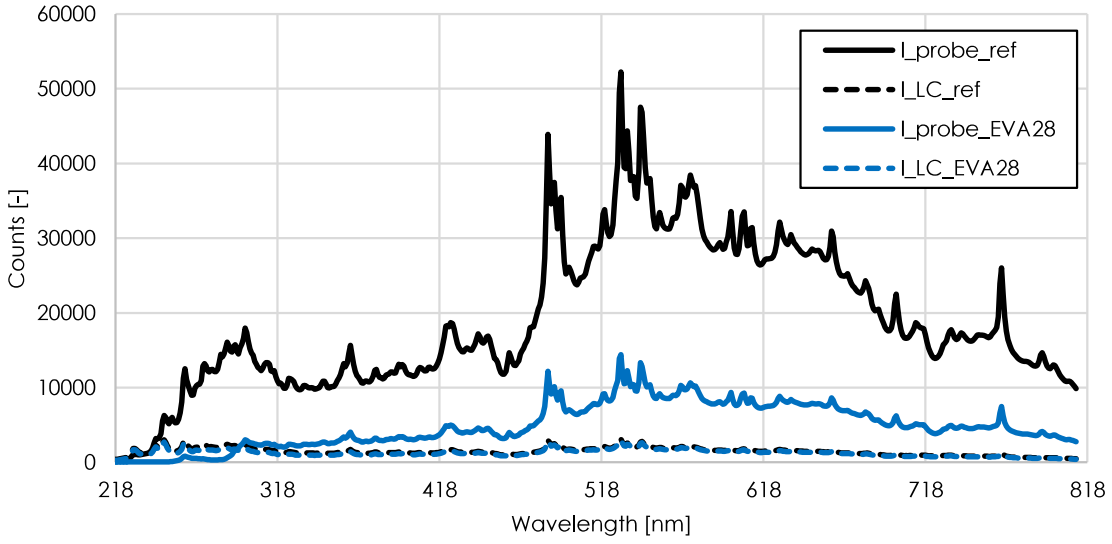

Fig. 5-8: Intensities of the probe signal and the light-compensation-channel signal for the reference material (air) and for EVA28. The signal of the LCs is nearly the same as it is not affected by the material (ET: 10 ms, NoF: 3).

In this way the corrected reference I_{ref}, sample I_s and dark standard I_{dark} is calculated in their respective measurement. Next the signal is converted to percent transmission or absorbance, according to Eq. (9) and (10). In Fig. 5-9 the corrected signals of the abovementioned probe and LC curves and the resulting transmission spectrum are shown.

$$T = 100 * \frac{I_s - I_{dark}}{I_{ref} - I_{dark}} \dots transmission\ [\%] \tag{9}$$

$$A = -\log\left(\frac{I_s - I_{dark}}{I_{ref} - I_{dark}}\right) \ldots absorbance \ [A.U.] \tag{10}$$

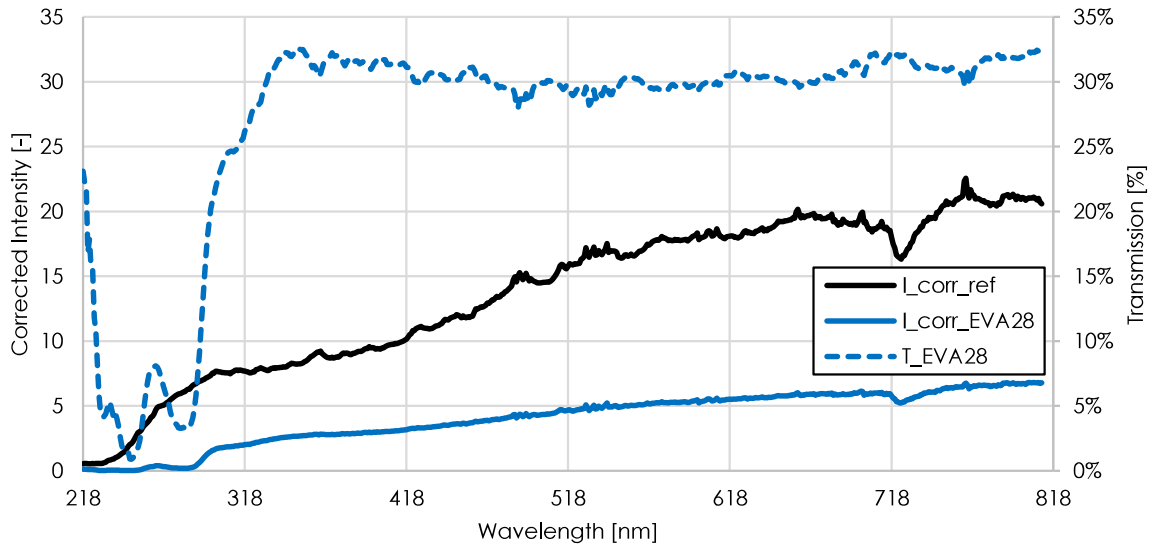

Fig. 5-9: Corrected reference and sample signal (primary axis) and the resulting transmission spectrum (secondary axis). The dark standard I_{dark} was neglected (ET: 10 ms, NoF: 3).

The required output format can be selected in the "Spec. Parameters" menu and the spectra can be saved as *.dat, *.spc and *.csv files. It is also possible to export the raw values from the sensor by recording in "Manual Operation" mode.

To smooth the results multiple exposures can be averaged to provide a single spectrum. The measurements in this thesis were recorded with 5 exposures per cycle.

5.2.1.5 Online Operation

After optimization and calibration, the spectra can be recorded in the "Online Operation" screen. It offers a comment function, configurable charts, start/stop and a small picture of the actual spectrum.

5.2.2 Sentronic SentroPAT

The Sentronic SentroPAT FO is a NIR process spectrometer ranging in wavelength between 1100 and 2200 nm. It comes with probes for powder measurements and one additional Dynisco reflection probe. For transmission measurements the ColVisTec UV/Vis probe were used as a makeshift. They have the same SMA905

connector, but due to incompatibilities they absorb some areas of the NIR range. The powder measurements (acting as a reference material) were done with the Sentronic SentroProbe DR LS reflectance probe.

5.2.2.1 Calibration

The calibration procedure is similar to the calibration of the UV/Vis spectrometer. At first the exposure time must be set to get around 50,000 to 55,000 counts intensity to prevent the sensor from oversaturating (The intensity resolution is 16 bit and similar to the InSpectroX). Then the reference spectrum was recorded. For transmission measurement the reference was air, for reflectance it was a white standard. In Fig. 5-10 and Fig. 5-11 the respective reference spectrum is depicted. It is readily identifiable that the transmission measurement wavelength range is interrupted due to incompatibilities with the UV/Vis probes. Therefore, the resulting spectra are only valid in the range from 1100 to 1350 nm and from 1450 to 1900 nm. The used configurations of the spectrometer are listed in Table 5-3.

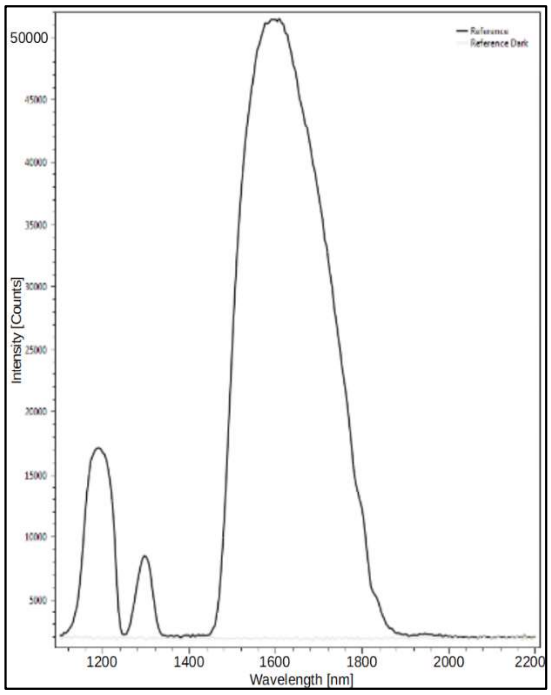

Fig. 5-10: Reference spectrum of air for transmission measurement with the ColVisTec probes.

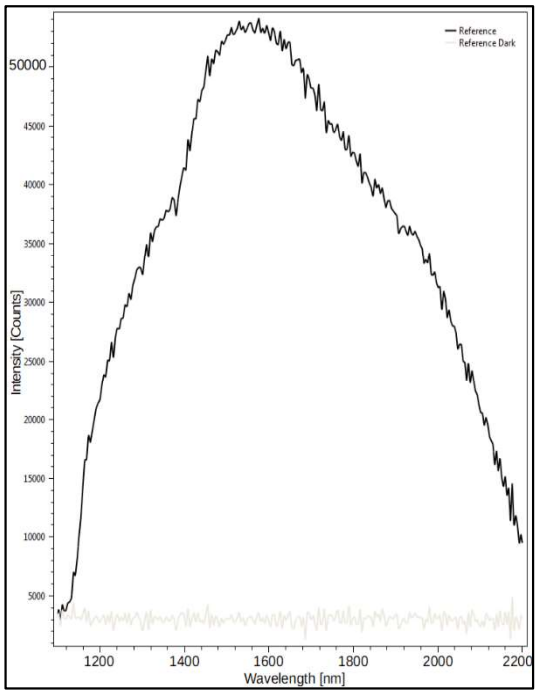

Fig. 5-11: Reference spectrum of the white standard for reflectance measurement with the reflection probe.

Table 5-3: Configuration of the Sentronic SentroPAT.

	Transmission	Reflectance
Exposure time	0.002 seconds	0.025 seconds
Averaged exposures	500	50
Resolution	1 nm	1 nm
Range	1100 – 1330 nm, 1470-1900 nm	1100 – 2200 nm

5.2.3 i-Raman® Plus BWS465-785

The i-Raman® Plus System is a portable Raman spectrometer covering a spectral range from 150 to 3350 cm^{-1}. Like the UV/Vis and the NIR spectrometer it has also an intensity resolution of 16 bit or 65,535 counts. The integration times range from 100 ms to 30 min, making it possible to measure very weak Raman signals. The spectrometer in combination with a special process probe, pictured in Fig. 5-12 and Fig. 5-13, was kindly provided by ColVisTec AG for the experiments at their headquarter with the configurations shown in Table 5-4.

Fig. 5-12: The i-Raman® Plus spectrometer by courtesy of ColVisTec AG.

Fig. 5-13: The laser trigger and the ColVisTec Raman probe built in the spectroscopy chamber.

Table 5-4: Configuration of the i-Raman® Plus.

	Reflectance
Exposure time	3 seconds
Averaged exposures	1
Excitation wavelength	785 nm
Range	150 – 3350 cm^{-1}

5.2.4 Shimadzu UV-2700 UV-VIS Spectrophotometer

The Shimadzu UV-2700, pictured in Fig. 5-14, is a laboratory transmission spectrophotometer capable of measuring absorptions up to 8 absorption units. Unlike the other spectrometers operating with process probes, this device measures the sample solution and the reference solution filled in the respective standard cuvette simultaneously. As there are no UV/Vis reference spectra in the literature for EVA28 the spectrum was obtained from a small strip, with a thickness of 0.98 mm, cut out of a pure EVA sheet prepared with the VCM tool. The strip is placed inside the standard cuvette with polished optical quartz windows, as seen in Fig. 5-15, and filled up with ethanol abs. against pure ethanol cuvette in the reference arm. The measurement was carried out in a range from 210 to 812 nm with a resolution of 0.5 nm.

Fig. 5-14: Shimadzu UV-2700 spectrophotometer.

Fig. 5-15: EVA28 strip in a standard cuvette filled up with ethanol.

6 Experimental Part

The main experimental part took place at the RCPE pilot plant in Graz/Austria. There the whole VCM Essentials for which the spectroscopy chamber is optimized and the ColVisTec UV/Vis spectrometer where available. At first, handling tests with pressure probes (instead of the spectroscopy probes) to investigate the assembling, disassembling and distance regulation behavior.

Furthermore, we got the opportunity to do some tests with the spectroscopy chamber at the ColVisTec headquarter in Berlin/Germany. Besides of the UV/Vis spectrometer they also had a Raman and a NIR spectrometer available.

Showing the possibilities of the chamber should be the main objective of the experimental part in this thesis. Therefore, all measurements use air as reference, so there is a primary standard for all materials.

6.1 Experiments to Characterize the Polymer Matrix

The following experiments were carried out without API only using the pure polymer. This chapter should show the general behavior of the spectra and the comparability with known references.

6.1.1 UV/Vis

The main spectroscopic method used in this thesis is UV/Vis. The following experiments should show up signal noise, impacts of different distances and an example of degradation.

6.1.1.1 Unfilled Chamber - Different Air Distances

The illuminating probe has a certain angle of the emitted light beam, forming a cone, even with the installed collimating lens. The total luminous flux is constant, so with increased distance the illuminance or flux per unit area is decreasing. Beer's law states the intensity decrease depending on the concentration and length, however the absorption because of the air does not play a role in this

analysis as it is transparent in the considered UV range. Fig. 6-1 shows a comparison of blank measurements at different distances, all normalized against a blank (air) measurement with a distance of 2 mm. As expected the 2 mm spectrum is a straight-line fluctuating around 100% transmission. The higher distance spectra have a wavelength dependent intensity drop.

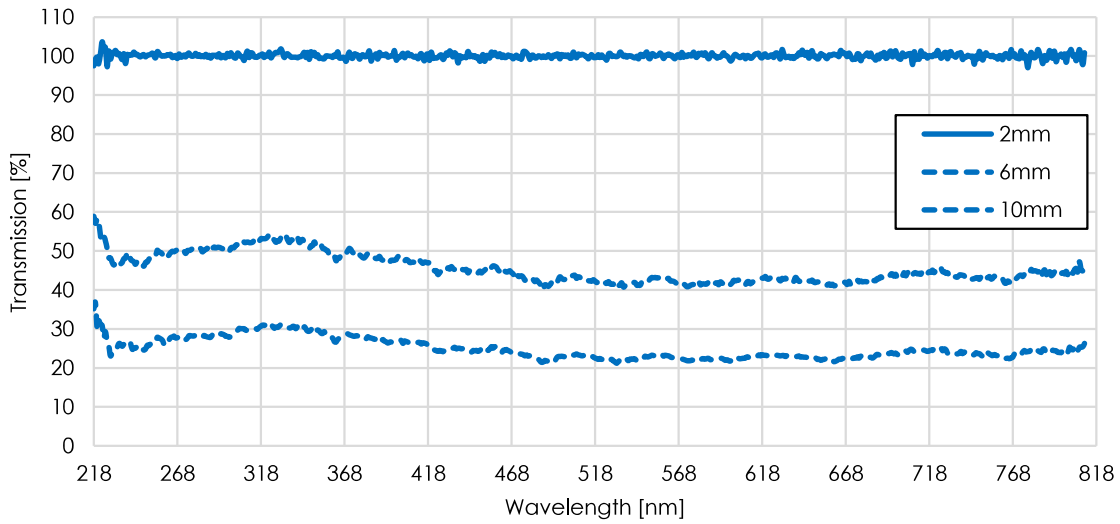

Fig. 6-1: UV/Vis blank measurement with calibration at 2mm distance (ET: 10 ms, NoF: 2).

If the light is properly focused by the probe lens to a straight beam, then the high transmission drop in combination with the strong wavelength dependency is unusual for a blank measurement. Though a properly focused beam wouldn't make much sense as it would drift due to the varying refractive indexes of different materials. It is not just that the refractive index depends on the material, but also on the wavelength of the light. Consequently, it is important to do a calibration for every preferred distance and the use of a divergent calibration distance is only suitable to a limited extend. It is also possible, that the probes pick up reflections from the chamber walls. For this case it would be helpful if the spectrometer software has the possibility to store different reference measurements and load them as required.

6.1.1.2 Noise of Reference Measurement

In Fig. 6-2 a comparison between the standard deviation of a blank spectrum and the corresponding raw lamp spectrum is shown. The calibration distance was

6.2 mm and the sample size include 20 spectra. There is a correlation between the height of the standard deviation and the lamps intensity. Especially in the far UV and generally in the upper and lower edge of the wavelength range the standard deviation rises. Because the noise under 250 nm rises far above the limit of 0.5% in subsequent experiments the selected wavelength range is between 250 and 800 nm.

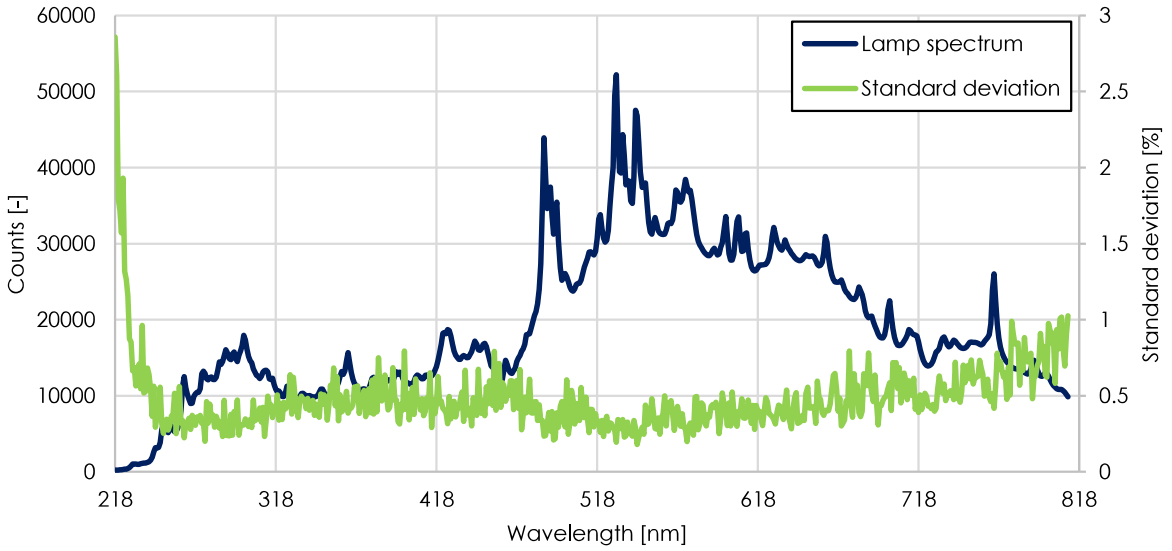

Fig. 6-2: Standard deviation of a blank measurement (20 spectra sample size) compared with the raw lamp spectrum (ET: 10 ms, NoF: 3).

6.1.1.3 Different Distances of EVA28 Sample in Comparison with Reference VCM Sample

One major feature of the spectroscopy chamber is the inline probe distance adjustment. With this it is possible to investigate how the spectrum reacts to a change in distance as seen in Fig. 6-3. The reference curve was measured according to chapter 5.2.4. Unsurprisingly, the amount of transmitted light decreases with higher distances. It must be noted that the calibration was performed at 2 mm distance, so there is some inaccuracy in the 5 and 10 mm spectra.

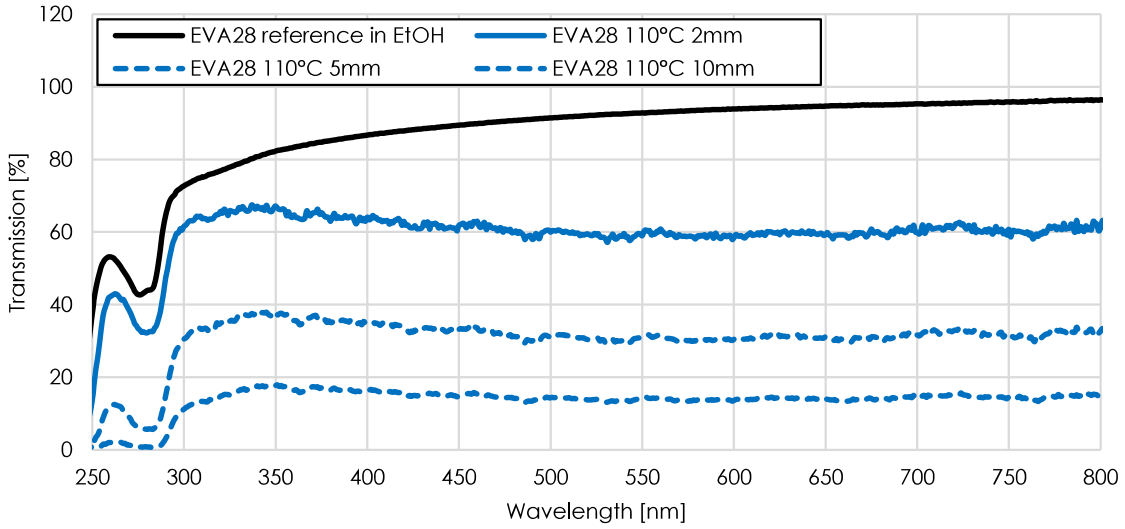

Fig. 6-3: EVA28 at different probe distances in comparison with reference spectrum from a VCM sample prepared in ethanol. Calibration at 2mm distance (ET: 10 ms, NoF: 2).

EVA28 has a characteristic absorption band at around 280 nm visible in the reference and in the spectroscopy chamber experiments. The slope difference above 300 nm of the reference can be attributed to refraction of the strip and difference of solid state and melt.

6.1.1.4 Stability of Eudragit® E PO

Doing stability measurements is one of the major advantages of the spectroscopy chamber. By varying temperature and measurement time degradation or dissolving processes can easily be captured and evaluated. To test the behavior of Eudragit® E PO some measurements were made at 170°C and afterwards the chamber was cooled down. The next day the material was heated up again to 170°C and then to 180°C. It kept at 180°C for another 15 minutes and was cooled down afterwards. In Fig. 6-4 spectra at 170°C before and after the cooldown and spectra at 180°C (initial and after 15min) are compared with each other.

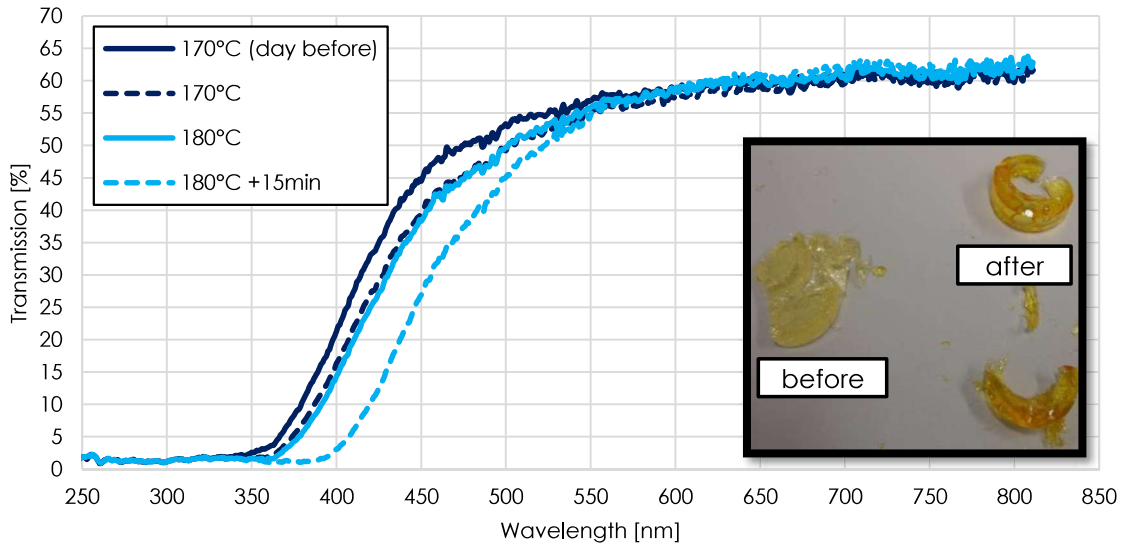

Fig. 6-4: UV/Vis stability experiment of Eudragit® E PO at 5 mm distance and how the sample looked alike after the experiment (ET: 10 ms, NoF: 4).

The whole cooldown and heat up (maximum temperature 170°C) lowered the transmission between 350 and 550 nm for 4 percentage points on average. Initially after rising the temperature to 180°C the spectra are constant. After an additional 15 minutes the spectra lowered by a further 7.6 percentage points. As expected the stressed sample looked more reddish afterwards, since the affected wavelengths from 350 to 550 nm represent blue and green light. Lin and Yu investigated the thermal stability of different methacrylates (Eudragit® L, S, L30D and carbopol polymers) by microscopic reflectance Fourier transform infrared spectroscopy. They found out that reactions occur at 170, 180, 183, 186°C and above depending on the used materials [30].

6.1.2 NIR Measurements with EVA28 and Eudragit® E PO

The available Dynisco compatible NIR probe at RCPE is a reflectance probe and is therefore not usable for transmission measurements. As a substitute the ColVisTec UV/Vis probes were used, which have the same SMA905 glass fiber connector. The fibers of the UV/Vis probe are not designed for the NIR range, so there are unwanted absorption bands in the NIR regime. In this setup, only wavelengths from 1100 to 1330 nm and from 1470 to 1900 nm are detectable in NIR transmission measurements. A reference spectrum of the powder was measured in

the laboratory with the SentroPAT system and reflection and transmission measurements in the chamber were done at molten state. The transmission measurements were carried out at 6.2mm probe distance. For more information see chapter 5.2.2.

Fig. 6-5 and Fig. 6-6 compare the reference spectrum of EVA28 and Eudragit® E PO powder with the reflection and transmission measurements of the molt. The rectangles indicate the wavelength ranges invisible for the ColVisTec transmission probes. For better readability there is a secondary axis providing a different scale for the absorption of the powder reference.

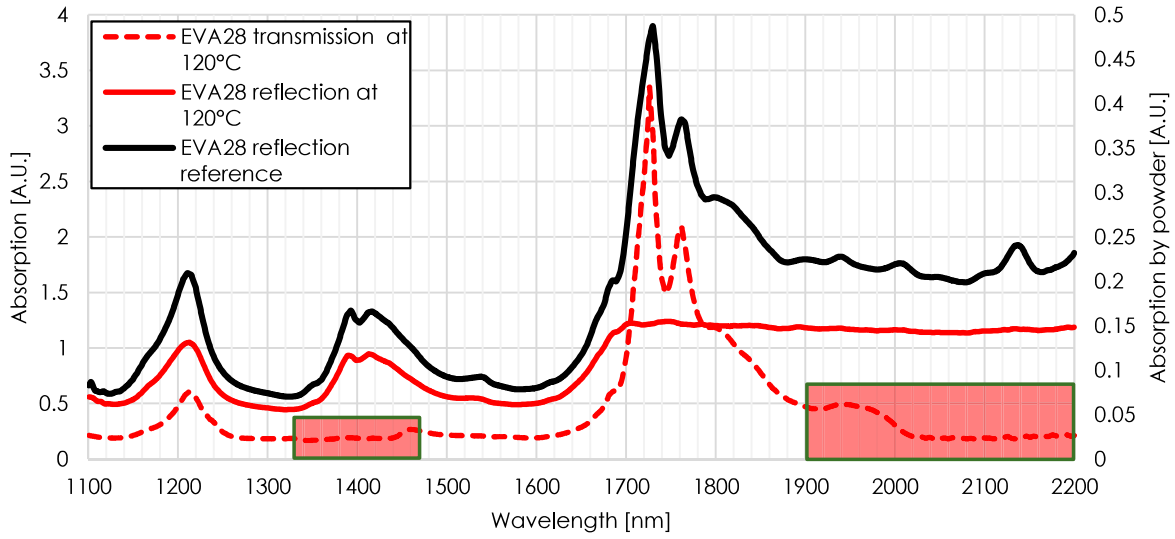

Fig. 6-5: NIR measurements from EVA28 in reflection and transmission mode. The secondary axis stands for the powder reference.

It is easily noticeable that the transmission spectra for both materials has no relevant peaks from 1330 to 1470 nm and over 1900 nm, as the used UV/Vis fibers are not transparent in this wavelength range. Despite of that the peaks at around 1200 nm and around 1750 nm are very characteristic and vary only a few nanometers between solid and molten state. Even the small steps at around 1700nm are clearly noticeable.

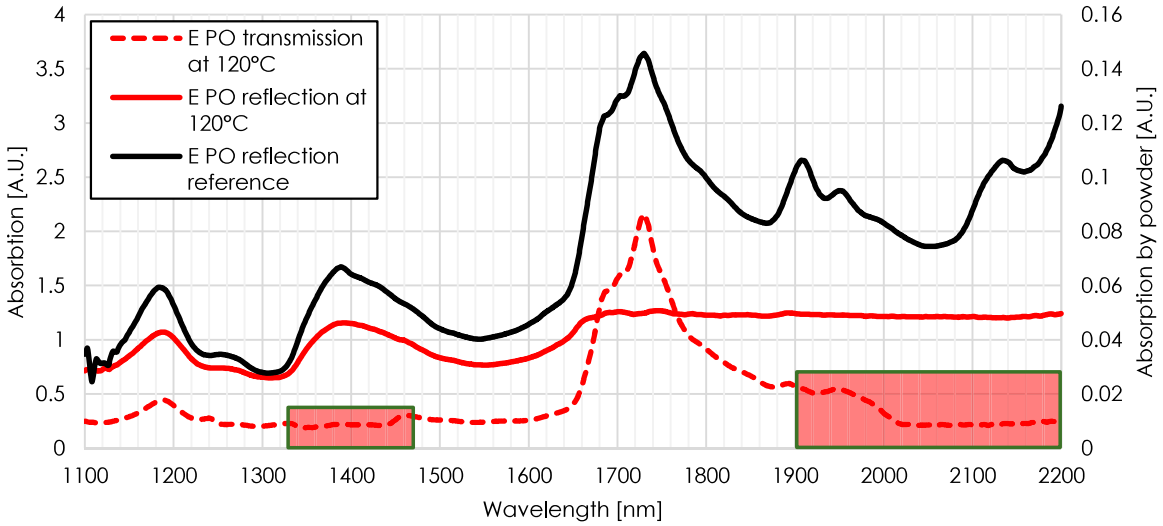

Fig. 6-6: NIR measurements from Eudragit® E PO in reflection and transmission mode. The secondary axis stands for the powder reference.

With the reflection probe it was even possible to show the absorption around 1400nm and a very small peak at 1540nm. The only problem with reflection measurements inside the chamber (when investigating translucent materials) is that there is no useful information above 1700nm and the spectrum varies with probe-to-wall distance. To investigate this behavior Fig. 6-7 compares the reflectance spectrum of 8mm and 11mm distance during measurement.

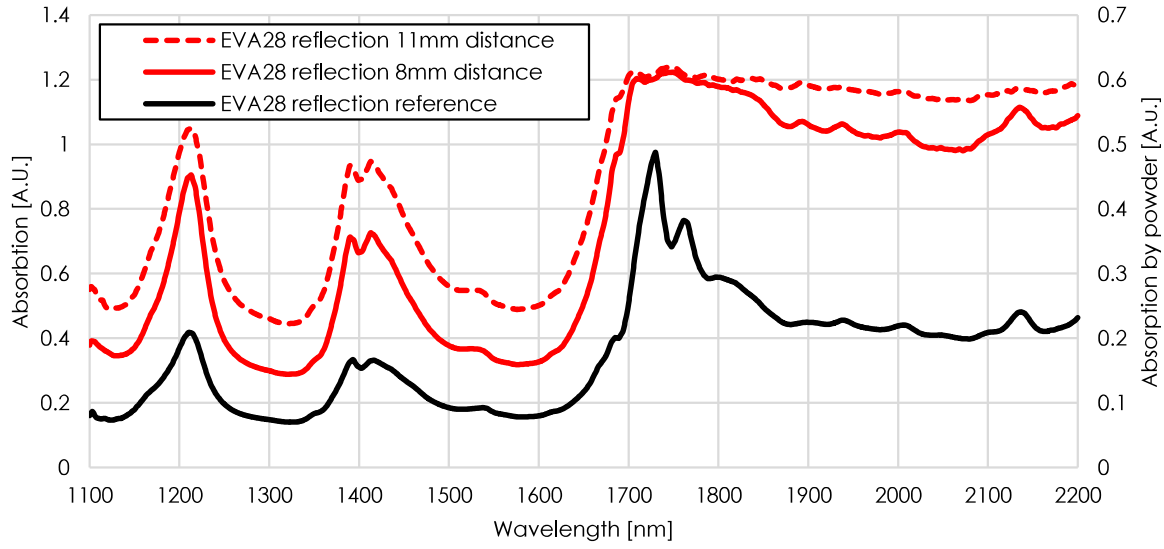

Fig. 6-7: NIR reflection measurements of EVA28 at 8 and 11mm probe-to-wall distance in comparison to the reference EVA28 powder.

As the absorbance rises with higher distance it is obvious that the light is rather reflected from the wall than from the material itself and works more like a transflectance measurement (were the foil on the other side of the wall acts like a mirror). From 1700 to 1800nm it seems like the polymer gets rather opaque (this is obvious as the absorption in this range is very high) and therefore no light or information is reflected. Over 1800nm the opacity lowers and at least at 8mm distance of the opposite wall the light reflected is high enough to differentiate easily between the characteristic absorption peaks.

In summary, it has been shown that the reflectance spectrum of molten samples in the chamber are in very good agreement to the powder reference up to a 1.2 A.U. threshold. This is the useful dynamic range of the chamber set up in reflectance mode. In transmission mode the useful dynamic range is over 2 A.U..

6.1.3 Raman Measurements with EVA28

The Raman measurements were carried out at the ColVisTec headquarter in Berlin/Germany. After the UV/Vis measurements the chamber was cooled down until the material inside was nearly solid. Then one probe was replaced by the Raman probe. The other one was closed by a cap after removing the fibers. Afterwards the chamber was heated up to 120°C and the spectra were recorded. For the sake of completeness, it needs to be said that the distance regulation has no influence on the Raman spectra as it is a surface sensitive method.The sample was EVA28 with a vinyl acetate amount of 28%. The measurements were carried out at different temperatures from molten to solid material (120°C and 40°C).

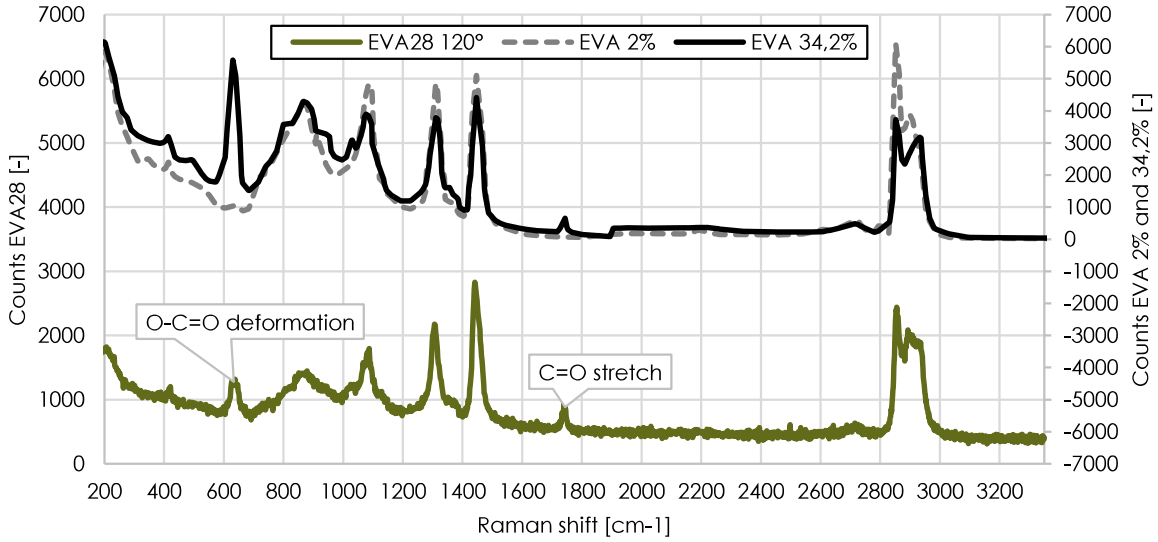

Fig. 6-8: Comparison of the background corrected EVA28 Raman spectra with Raman measurements of EVA with 2% and 34,2% VA content taken from a publication of Kaiser Optical Systems, Inc. measured in an extrusion process at 180°C [31]

As seen in Fig. 6-8 the characteristic peaks of the recorded EVA28 spectra are similar to the ones found in a publication of Kaiser Optical Systems. According to their publication [31] there are characteristic VA bands at 630 cm^{-1} and 1740 cm^{-1} also seen in the measurements of EVA28 taken in the spectroscopy chamber. They do not occur on the EVA 2% curve except of a small peak at 630 cm^{-1}.

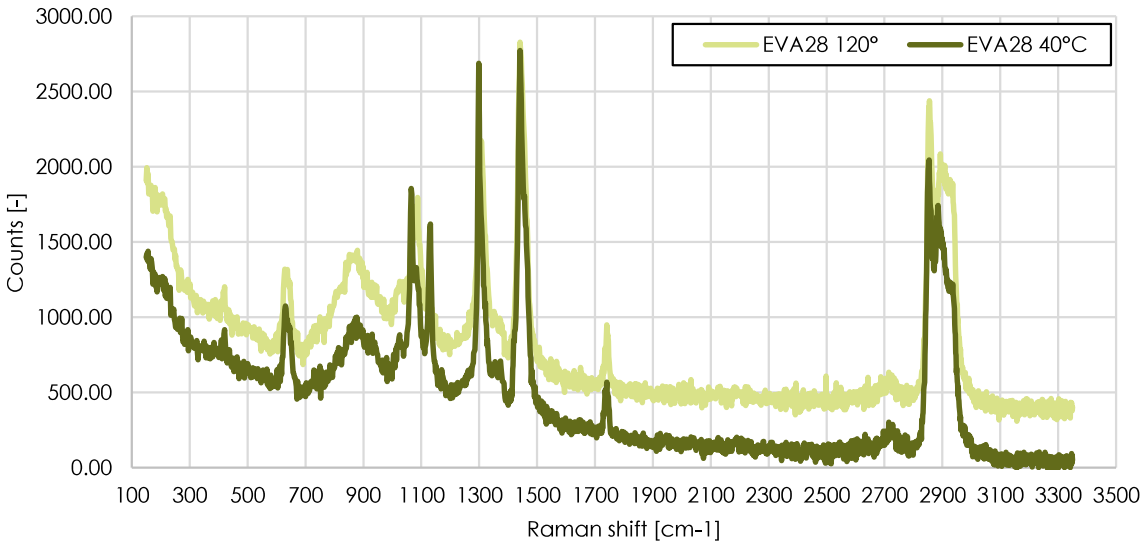

Fig. 6-9: Comparison of EVA28 at 120°C and EVA28 at 40°C

The temperature (or state of matter) also has an influence on the spectra as can be seen in Fig. 6-9. From 120°C to 40°C major differences appear as risen bands at 1067, 1130 and 1298 cm^{-1} and as lowered bands at around 872, 1023 and 2925 cm^{-1} as well as a slightly changed Raman shift of some peaks (1067 and 1298 cm^{-1}). Also, the overall background noise rises with temperature.

6.2 Experiments with Polymer Matrix and Added API

Experiments with API were mainly carried out with Estriol in EVA28 in different concentrations. This setup should prove the capability of detecting API in the chamber and to build a chemo-metric model out of the resulting data.

6.2.1 Estriol in EVA28

To prevent drug carry-over the experiments were carried out from lowest to highest API content, from 0 to 8.48%. However, 8.48% was not measurable because the maximum solubility of the API is around ~4% in the matrix at process conditions and therefore the precipitated crystals blocked the transmission of the light. After the measurements the samples were analyzed with HPLC to get the exact API content and exclude errors made in the dilution series. As it can be seen in Fig. 6-10 the raising API content is easily noticeable in the UV range between 250 and 370nm, but contrary to expectations in all spectra greater or equal 0.17% API an inexplicable double peak appeared. For determining the absorbance, the averages of 20 transmission spectra in each concentration were converted according to Eq. (11).

$$A(\lambda) = -\log\left(\frac{T_i(\lambda)}{T_{pure}(\lambda)}\right) \tag{11}$$

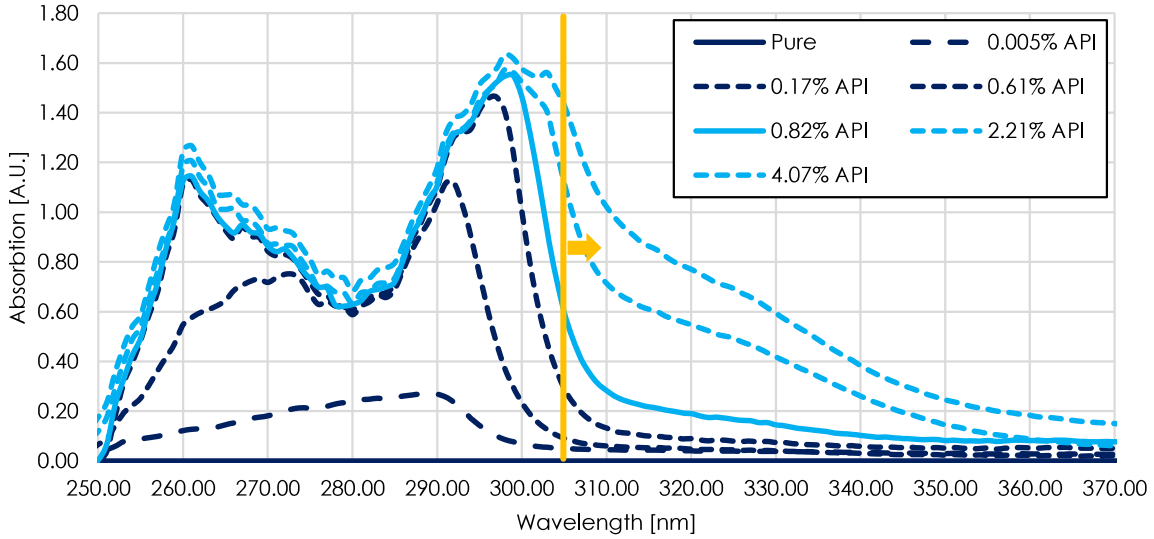

Fig. 6-10: Absorption spectra of different Estriol concentrations in EVA28 at 6.2mm probe distance measured in transmission mode (ET: 10 ms, NoF: 3). The vertical line indicates the lower border used for the chemo-metric model.

As it can be seen in Fig. 6-11, Estriol and EVA both have an absorption maximum around 280nm. So, there is the assumption that the higher concentrated formulations cannot be measured by the UV VIS spectrometer.

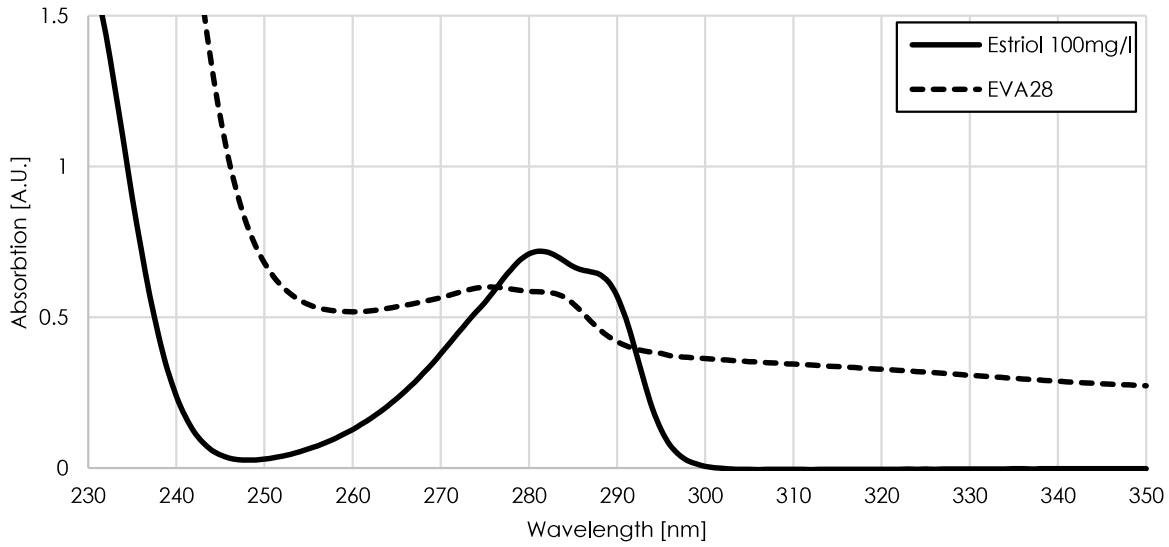

Fig. 6-11: Absorption spectra of estriol 100mg/l and EVA28 VCM sample in ethanol in a standard cuvette.

Based on Beer's law, the absorption coefficient can be calculated according to Eg. (12). The probe distance l is 0.62 cm, the molar mass (M_{E3}) is 288 g/mol and the

density (ρ_{EVA28}) is 950 g/l. The mass fraction x_{E3} depends on the experiment. In Fig. 6-12 the molar absorption coefficient calculated from measurements of a reference solution (100 mg/l E3 in a cuvette with l = 1 cm) and of the spectroscopy chamber experiments can be seen. The 0.005% API result corresponds well with the reference measurement and can therefore be assumed as correct, but all the other results calculate far too low.

$$\varepsilon(\lambda) = \frac{A(\lambda)}{l * c_{E3}} = \frac{A(\lambda) * M_{E3}}{l * x_{E3} * \rho_{EVA28}} \tag{12}$$

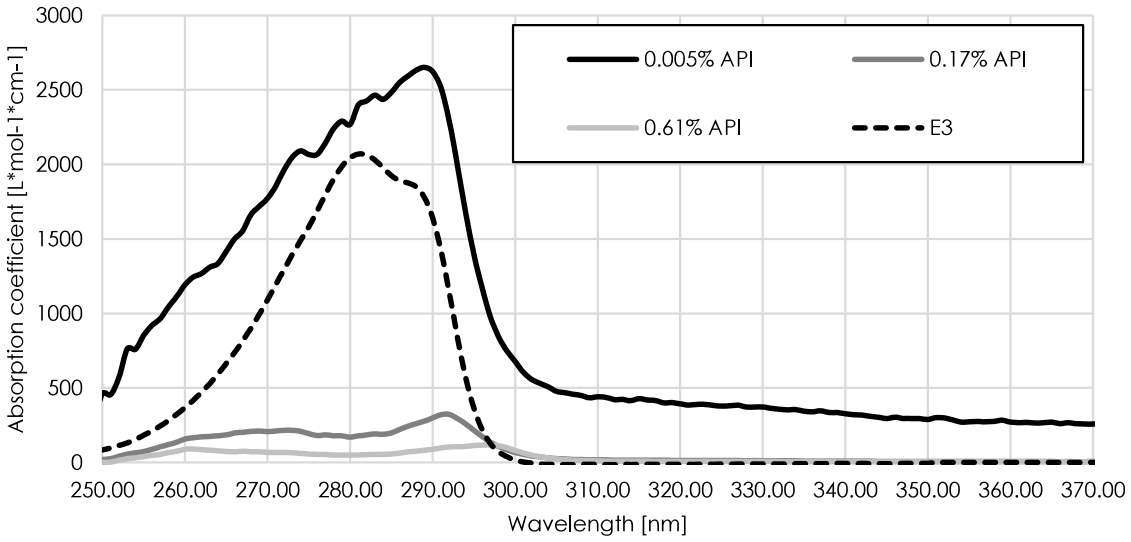

Fig. 6-12: Molar absorption coefficient determined from E3 in solution (100 mg/l) and from the three lower concentrated results of the experiments in the spectroscopy chamber.

To describe the distorted curves of the higher concentrated formulations one should calculate the expected absorption of the 0.17% API curve. With a molar absorption coefficient of 2070 L*mol-1*cm-1 this would mean an absorption of around 7.5 based on Beer's law. Since in the pure EVA28 the transmission in this wavelength range is around 3% the overall light passing through is reduced by 10^9 (9 absorption units!). This is far outside the detection limit of the spectrometer (as a reminder, the Shimadzu spectrophotometer has a detection limit of maximum 8 A.U. under special set-up conditions, e.g. extended scanning time and installed

double monochromator). As can be seen in Fig. 6-10 the higher concentrations form a band, giving the dynamic limit of the set-up. The dynamic range is about 1.4 a.u. at 300 nm and lowers to 0.6 a.u. at 280 nm. The range goes up a little bit again before it declaims to essentially zero at 250 nm. Outside of this range no measurements are valid in this UV regime. This gives a natural limit on the detectable concentration by direct evaluation of the substances peak. In this configuration with a detection limit of 0.6 A.U. at 280 nm wavelength the maximum fully measurable concentration of estriol would have been about 0.014%.

To enhance the upper detection limit, a possible way is to calibrate the spectrometer to the pure polymer instead of air and only in the UV active range of the API (from 250 to 300nm) where the overall transmission is much lower than in the visible range and practically oversaturating the spectra in all other parts. We have investigated analogical results with another, similar acting API in extruder measurements. This shows again the usefulness of the invented chamber. An expensive extruder run could have been prevented by testing the formulation first in the spectroscopy chamber and adjust the calibration of the spectrometer based on this knowledge.

6.2.1.1 Chemo-metric model

According to Beer's law (see chapter 2.1) the API content is proportional to the height of the absorption peak. This only holds in the linear region of the spectrometer. As mentioned above the resulting spectra of our test series have distorted curves in the higher API contents, because the limitations of the ColVisTec spectrometer were reached. The interesting question is: Could the spectra far outside the characteristic absorption peaks, which are again in the linear regime of the spectrometer be used to form a new type of chemo-metric model?

The following points are in favor of this proposition

- There is no counterargument that Beer's law is not valid in the tails of peaks
- There is no varying line broadening mechanism involved between spectra, e.g., temperature and pressure kept constant

- The optical properties are not changing between samples. If the solubility limit is reached, the API precipitates. The generated crystals in the melt induce scatter, which translated to additional absorption because the effective light path length is higher. This also points to a spectroscopic method to monitor crystal growth.

Model development

Since the information lays in the tail of the peak it is obvious to use only the integral from 305nm and upwards also seen in Fig. 6-10 indicated as the vertical line. The used model is defined by Eq. (13).

$$x_{API} = |a * S + b| \tag{13}$$

with x as the API content in [%], S as the Area under the absorption spectra and a as a parameter. The linear regression was fitted in Excel.

As seen in Fig. 6-13, the assumption that the API content is proportional to the area under the absorption curve is true.

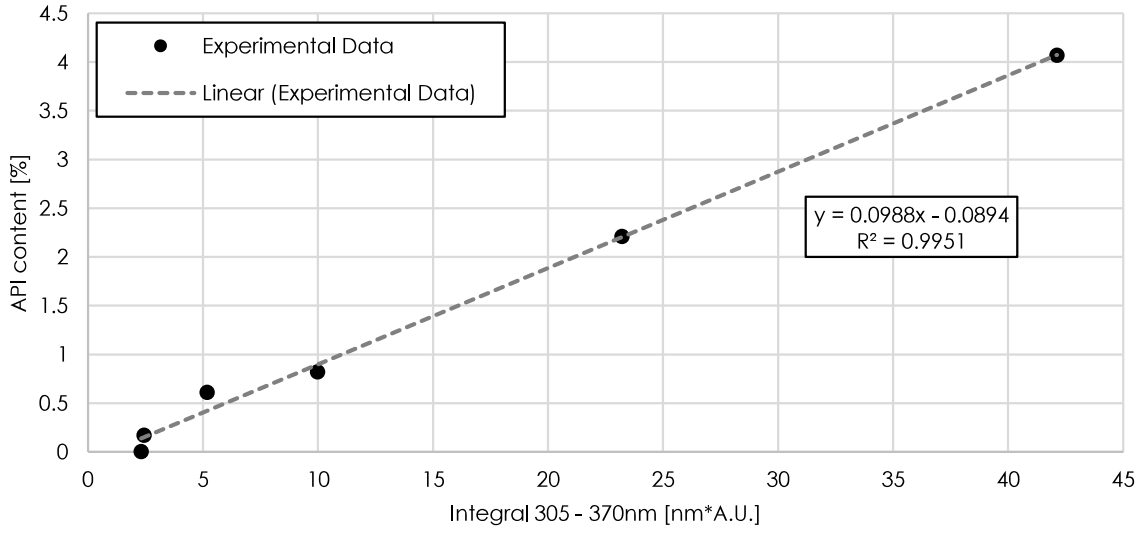

Fig. 6-13: API content over the integrated absorption spectra from 305 to 370nm. Approximation of Eq. (13) is made in Excel 2016 and gives a = 0.0988, b = -0.0894 and R^2 = 0.9951.

Table 6-1: Data used for chemo-metric model

API content [%]	API content calc. [%.]	Area under curve [nm*A.U.]
0	0.089	0
0.005	0.139	2.312
0.17	0.151	2.434
0.61	0.423	5.184
0.82	0.896	9.976
2.21	2.204	23.21
4.07	4.072	42.12

This follows Beer's law, since if we integrate Beer's law after the wavelength we get

$$\int_{\lambda_1}^{\lambda_2} A(\lambda)\, d\lambda = \int_{\lambda_1}^{\lambda_2} \varepsilon(\lambda) * c_{E3} * l\, d\lambda = c_{E3} * l * \int_{\lambda_1}^{\lambda_2} \varepsilon(\lambda) d\lambda = c_{E3} * k$$

As ε is independent from the concentration c_{E3} and the path length l the concentration can be described as follows in Eq. (14) and is therefore proportional to the sum of the discrete absorption values.

$$c_{E3} = \frac{\int_{\lambda_1}^{\lambda_2} A(\lambda)\, d\lambda}{k} = a * \sum_{\lambda_1}^{\lambda_2} A(\lambda) = a * S \tag{14}$$

7 Conclusion

The aim of this thesis was to engineer and validate a new way to design and calibrate spectroscopic PAT tools in the field of pharmaceutical HME. Therefore, common spectroscopic methods like UV/Vis, Raman and NIR were used to investigate the spectra of different polymers.

The tool itself consists of few parts and is designed as simple as possible. After some practicing it is easy to assemble all parts and fill up the starting material. Main functions are the temperature and distance variability during a single experiment, which both are in good working order. The cleaning procedure is very straightforward because of installed separation foils which are a technology adapted from the VCM tool.

Two main materials were used in the validation experiments, EVA28 and Eudragit® E. Both polymers are translucent and measurable in transmission mode. It was possible to recognize an unspecified degradation process on Eudragit® E at 180°C with UV/Vis spectroscopy, which resulting color change is also identifiable by eye. With NIR and Raman spectroscopy both materials have similar characteristic peaks to the known reference. It was even possible to see differences between solid and molten state in the Raman spectrum.

In the pharmaceutical field almost all polymers are used as a matrix for an embedded API. Estriol in EVA28 in different concentrations was used in combination with UV/Vis spectroscopy as a testing setup. It was possible to detect an API content starting from 0.005% up to 4.07%. Higher concentrated mixtures got too opaque to measure in transmission mode due to precipitation of the API. According to Beer's law the height (and the integral) of the absorption curve should be proportional to the API content. This was proved by a linear regressed chemometric model and by the resulting coefficient of determination (R^2) of 99.51%.

The spectroscopy chamber can be used with all spectroscopy methods providing probes with the standard Dynisco thread used in common extruders.

8 References

[1] P. R. Wahl, D. Treffer, S. Mohr, E. Roblegg, G. Koscher, and J. G. Khinast, "Inline monitoring and a PAT strategy for pharmaceutical hot melt extrusion," *Int. J. Pharm.*, vol. 455, no. 1–2, pp. 159–168, 2013.

[2] P. Hitzer *et al.*, "Process analytical techniques for hot-melt extrusion and their application to amorphous solid dispersions," *Anal. Bioanal. Chem.*, vol. 409, no. 18, pp. 4321–4333, 2017.

[3] D. Treffer, A. Troiss, and J. Khinast, "A novel tool to standardize rheology testing of molten polymers for pharmaceutical applications," *Int. J. Pharm.*, vol. 495, no. 1, pp. 474–481, 2015.

[4] B. Valeur and M. N. Berberan-Santos, *Molecular Fluorescence*, Second Edi. Weinheim, Germany: Wiley-VCH Verlag GmbH & Co. KGaA, 2012.

[5] W. W. Parson, *Modern Optical Spectroscopy*. Berlin, Heidelberg: Springer Berlin Heidelberg, 2007.

[6] S. Behera, S. Ghanty, F. Ahmad, S. Santra, and S. Banerjee, "UV-Visible Spectrophotometric Method Development and Validation of Assay of Paracetamol Tablet Formulation," *J. Anal. Bioanal. Tech.*, vol. 3, no. 6, 2012.

[7] K. A. Bakeev, *Process Analytical Technology: Spectroscopic Tools and Implementation Strategies for the Chemical and Pharmaceutical Industries: Second Edition*. Chichester, UK: John Wiley & Sons, Ltd, 2010.

[8] L. Saerens *et al.*, "In-line NIR spectroscopy for the understanding of polymer-drug interaction during pharmaceutical hot-melt extrusion," *Eur. J. Pharm. Biopharm.*, vol. 81, no. 1, pp. 230–237, 2012.

[9] L. Saerens *et al.*, "In-line solid state prediction during pharmaceutical hot-melt extrusion in a 12 mm twin screw extruder using Raman spectroscopy," *Eur. J. Pharm. Biopharm.*, vol. 87, no. 3, pp. 606–615, 2014.

[10] Specac Ltd, "Product Catalogue 2016-17." Orpington, pp. 3–148, 2016.

[11] ColVisTec AG, "Quality by Design: Integrating PAT Measurement in Hot Melt Extrusion." Berlin-Adlershof, p. 59, 2016.

[12] F. Wülfert, W. T. Kok, and A. K. Smilde, "Influence of Temperature on Vibrational Spectra and Consequences for the Predictive Ability of Multivariate Models," *Anal. Chem.*, vol. 70, no. 9, pp. 1761–1767, 1998.

[13] D. Cozzolino *et al.*, "Effect of temperature variation on the visible and near infrared spectra of wine and the consequences on the partial least square calibrations developed to measure chemical composition," vol. 588, pp. 224–230, 2007.

[14] A. Zosel, "Der Schubmodul von Hochpolymeren als Funktion von Druck und Temperatur," *Kolloid-Zeitschrift und Zeitschrift für Polym.*, vol. 199, no. 2, pp. 113–125, Oct. 1964.

[15] "getAMO Ltd." [Online]. Available: http://www.getamo.com/www/getspec.nsf/main.html?open&lang=EN&id=getProbe_DR_NIR_Dynisco_EN. [Accessed: 17-Aug-2018].

[16] Picture: Josell7, "Optical reflection: critical angle and total internal reflection," *CC BY-SA 3.0*. [Online]. Available: https://commons.wikimedia.org/wiki/File:RefractionReflextion.svg. [Accessed: 28-Aug-2018].

[17] Picture: User A1, "Illustration of the Numerical aperture for an Optic fibre," *CC BY-SA 3.0*. [Online]. Available: https://commons.wikimedia.org/wiki/File:Optic_fibre-numerical_aperture_diagram.svg. [Accessed: 28-Aug-2018].

[18] A. L. Kelly, S. A. Halsey, R. A. Bottom, S. Korde, T. Gough, and A. Paradkar, "A Novel Transflectance Near Infrared Spectroscopy Technique for Monitoring Hot Melt Extrusion," *Int. J. Pharm.*, vol. 496, pp. 117–123, 2015.

[19] F. C. Clarke, S. V. Hammond, R. D. Jee, and A. C. Moffat, "Determination of the information depth and sample size for the analysis of pharmaceutical materials using reflectance near-infrared microscopy," *Appl. Spectrosc.*, vol.

56, no. 11, pp. 1475–1483, 2002.

[20] S. G. Hatzikiriakos, “Wall slip of molten polymers,” *Prog. Polym. Sci.*, vol. 37, no. 4, pp. 624–643, Apr. 2012.

[21] W. Michaeli, *Extrusion Dies for Plastics and Rubber*, vol. 30, no. 2. München: Carl Hanser Verlag GmbH & Co. KG, 2003.

[22] D. Kreutz, J. Yu, P. Esteves-Verissimo, C. Magalhaes, and F. M. V. Ramos, “The KISS principle in Software-Defined Networking: An architecture for Keeping It Simple and Secure,” 2017.

[23] Dynisco, “Mounting Hole Details.” p. 1.

[24] R. Rowe, P. Sheskey, and M. Quinn, “Handbook of Pharmaceutical Excipients,” *Handb. Pharm. excipients, Sixth Ed.*, pp. 549–553, 2009.

[25] “Ethylene-vinyl acetate copolymer,” *CC-Zero*. [Online]. Available: https://commons.wikimedia.org/wiki/File:Ethylen-Vinylacetat.svg.

[26] “Polymethylmethacrylate,” *CC-Zero*. [Online]. Available: https://commons.wikimedia.org/wiki/File:Polymethylmethacrylat.svg.

[27] E. S. Ali, C. Mangold, and A. N. Peiris, “Estriol,” *Menopause*, vol. 24, no. 9, pp. 1081–1085, Sep. 2017.

[28] “Estriol,” *Public domain*. [Online]. Available: https://commons.wikimedia.org/wiki/File:Estriol.svg.

[29] ColVisTec AG, “InSpectro X - Manual,” Rev. 1.3.

[30] S. Y. Lin and H. L. Yu, “Thermal stability of methacrylic acid copolymers of Eudragits L, S, and L30D and the acrylic acid polymer of carbopol,” *J. Polym. Sci. Part A Polym. Chem.*, vol. 37, no. 13, pp. 2061–2067, 1999.

[31] Kaiser Optical Systems Inc., “Kaiser ’ s RamanRxn3 ™ Analyzer for In - line Monitoring of Ethylene Vinyl Acetate Copolymer with Raman Spectroscopy,” pp. 1–8, 2014.